DRAFT FOR THE JOURNAL OF GEOPHYSICAL RESEARCH

Quantifying Parameter Sensitivity, Interaction and Transferability in Hydrologically Enhanced Versions of Noah-LSM over Transition Zones

ENRIQUE ROSERO,[1] ZONG-LIANG YANG,[1] THORSTEN WAGENER,[2] LINDSEY E. GULDEN,[1] SONI YATHEENDRADAS,[3,4] and GUO-YUE NIU[1]

[1]*Department of Geological Sciences, Jackson School of Geosciences, The University of Texas at Austin, Austin, Texas, USA*

[2]*Department of Civil and Environmental Engineering, The Pennsylvania State University, University Park, Pennsylvania, USA*

[3]*NASA Goddard Space Flight Center, Hydrological Sciences Branch, Greenbelt, Maryland, USA*

[4] *Earth System Science Interdisciplinary Center, University of Maryland, College Park, Maryland, USA*

Manuscript submitted 10 March 2009

Corresponding author address:
Zong-Liang Yang,
1 University Station #C1100,
The University of Texas at Austin,
Austin, TX 78712-0254.
E-mail: liang@jsg.utexas.edu

ABSTRACT

We use sensitivity analysis to identify the parameters that are most responsible for shaping land surface model (LSM) simulations and to understand the complex interactions in three versions of the Noah LSM: the standard version (STD), a version enhanced with a simple groundwater module (GW), and version augmented by a dynamic phenology module (DV). We use warm season, high-frequency, near-surface states and turbulent fluxes collected over nine sites in the US Southern Great Plains. We quantify changes in the pattern of sensitive parameters, the amount and nature of the interaction between parameters, and the covariance structure of the distribution of behavioral parameter sets. Using Sobol's total and first-order sensitivity indexes, we show that very few parameters directly control the variance of the model output. Significant parameter interaction occurs so that not only the optimal parameter values differ between models, but the relationships between parameters change. GW decreases parameter interaction and appears to improve model realism, especially at wetter sites. DV increases parameter interaction and decreases identifiability, implying it is overparameterized and/or underconstrained. A case study at a wet site shows GW has two functional modes: one that mimics STD and a second in which GW improves model function by decoupling direct evaporation and baseflow. Unsupervised classification of the posterior distributions of behavioral parameter sets cannot group similar sites based solely on soil or vegetation type, helping to explain why transferability between sites and models is not straightforward. This evidence suggests a priori assignment of parameters should also consider climatic differences.

Key words: sensitivity analysis, land surface models, Noah LSM, model identification

Index terms: 1843 Land/atmosphere interactions, 1805 Computational hydrology, 0550 Model verification and validation, 1873 Uncertainty assessment, 1847 Modeling

1. Introduction

Like other environmental models built to support scientific reasoning and testable hypotheses to improve our understanding of the Earth system, land-surface models (LSMs) have grown in sophistication and complexity (Pitman, 2003; Niu et al., 2009). The evaluation of LSM simulations is consequently non-trivial and, especially when LSMs are to be used in predictive mode for operational forecasting, policy assessments, or decision making, demands more powerful methods for the analysis of their behavior (Saltelli, 1999; Jakeman et al., 2006; Randall et al., 2007; Gupta et al., 2008; Abramowitz et al., 2009). One such method is sensitivity analysis (SA), which is the process of investigating the role of the various assumptions, simplifications and other input (parameter) uncertainties in shaping the simulations made by a model. SA is a tool that enables exploring high-dimensional parameter spaces of complex environmental models to better understand what controls model performance (Saltelli et al., 2008). Monte Carlo-based uncertainty and SA uses the results of multiple model realizations to evaluate the range of model outcomes and identifies the input parameters that give rise to this uncertainty (Wagener et al., 2001; Wagener and Kollat, 2007). Used to its full potential, SA weighs model adequacy and relevance, identifies critical regions in the space of the inputs, unravels parameter interactions, establishes priorities for research, and, through an interactive process of revising the model structure, leads to simplified models and increased understanding of the natural system (Saltelli et al., 2006). In this article, we inform LSM development by using sophisticated SA to guide the development of the commonly used Noah LSM (Ek et al., 2003).

SA has been an underutilized resource in LSM development. Approaches to quantify 'sensitivity' (the rate of change in model response with respect to a factor) have very frequently been restricted to a simple exploratory analysis of the effects of factors taken one-at-a-time

(OAT), without regard for interactions between factors. Such factors can be parameters (e.g., Pitman, 1994; Gao et al., 1996; Chen and Dudhia, 2001; Trier et al., 2008), meteorological forcing, or ancillary data sets (e.g., Kato et al., 2007; Gulden et al., 2008a). OAT is illicit and unjustified for non-linear models (Saltelli, 1999; Bastidas et al., 1999; Saltelli et al., 2006). More powerful and sophisticated approaches that account, explicitly or implicitly, for parameter interactions include the factorial method (e.g., Liang and Guo, 2003; Oleson et al., 2008) and regionalized sensitivity analysis (RSA) (e.g., Bastidas et al., 2006, Demaria et al., 2007; Prihodko et al., 2008). The factorial method is a global variance-based sensitivity analysis (VSA) in which a selected number of model runs whose parameters have been perturbed by an arbitrary percent from an arbitrary reference value (default) are evaluated to identify parameters that affect the variance of the model output and to calculate a rough estimate of the low-order interactions. RSA, on the other hand, representatively samples the entire parameter space and provides a more robust assessment of the way in which parameter distributions change between subjectively defined 'good' and 'bad' (i.e., behavioral and non-behavioral) model simulations. RSA does not explicitly account for interactions between parameters and is typically applied with the sole purpose of identifying sensitive parameters to reduce the dimensionality of the calibration problem (e.g., Bastidas et al., 1999). When RSA and VSA are used separately, both the lack of firm conclusions regarding the effect of dominant parameters (and their interactions) on the output (e.g., Bastidas et al., 2006) and the inability to draw cause-effect relationships between parameter regions and model responses (e.g., Liang and Guo, 2003) have precluded SA findings from being widely used in model development. Our approach complements the information about the posterior distributions of behavioral parameters (RSA) with information about their contributions to model variance (VSA). The Monte Carlo-based VSA that we use (the method of

Sobol') is more robust than factorial analysis because it employs a representative sample of parameter space and bypasses the perceived 'complexities' often associated with powerful SA methods.

Our SA guides the investigation of the performance and physical realism of three versions of the Noah LSM: the standard Noah (STD), a version augmented with a simple groundwater model (Niu et al., 2007) (GW), and a version augmented with an interactive canopy model (Dickinson et al., 1998) (DV). We evaluate the performance of Noah LSM in simulating the land-surface states and fluxes at nine sites in a transition zone between wet and dry climates using the datasets of IHOP_2002 (LeMone et al., 2007). Because of the strength of the land-atmosphere coupling in transition zones (Koster et al., 2004), our work focuses on warm-season climates of the US Southern Great Plains. We document how parameter interaction and sensitivity varies with model, site, soil, vegetation, and climate. We investigate the ways in which alternate model structures affect the behavior of 'physically meaningful' LSM parameters, focusing on the dominant parameter interactions that dictate model response. We show that only a few parameters directly control model variance and that parameter interaction is significant. We further compare the similarity of estimated multivariate posterior distributions of behavioral parameters and their sensitivity against those obtained at other sites. We show that the changes between sites are not solely controlled by soil or vegetation types but appear to be strongly related to the climatic gradient.

This paper is organized as follows. Datasets, models, and methods are described in section 2. Experimental design and driving questions are formulated in section 3. Section 4 presents the patterns of sensitivity obtained via RSA and the global variance-based method of Sobol'. Section 5 presents a case study demonstrating the use of SA to understand the functional relationships between behavioral parameters, whose interaction serves to characterize model structure and test hypotheses that regard the formulation of model. Section 6 discusses implications of the results for the transferability of parameters between locations with similar physical characteristics. Conclusions are summarized in section 7.

2. Models, data and methods

2.1. Hydrologically enhanced versions of Noah LSM

We compare the standard Noah LSM release 2.7 (STD) to a version that we equipped with a short-term phenology module (DV) and one that couples a lumped, unconfined aquifer model to the model soil column (GW).

2.1.1. Noah standard release 2.7 (STD)

Noah (Ek et al., 2003; Mitchell et al., 2004) is a one-dimensional, medium complexity LSM used in operational weather and climate forecasting. The model is forced by incoming short- and longwave radiation, precipitation, surface pressure, relative humidity, wind speed and air temperature. The computed state variables include soil moisture and temperature, water stored on the canopy and snow on the ground. Prognostic variables include turbulent heat fluxes, and fluxes of moisture and momentum. Noah has a single canopy layer with climatologically prescribed albedo and vegetation greenness fraction. The soil profile of Noah is partitioned into 4 layers (lower boundaries at 0.1, 0.4, 1.0 and 2.0 m below the surface). The vertical movement of water is governed by mass conservation and a diffusive form of the Richard's equation. Infiltration is represented by a conceptual parameterization for the subgrid treatment of precipitation and soil moisture. Drainage at the bottom is controlled only by gravitational forces; percolation neglects hydraulic diffusivity. Direct evaporation from the top soil layer, from water intercepted by the canopy and adjusted potential Penman-Monteith transpiration are combined to represent total evapotranspiration. The surface energy balance determines the skin temperature of the combined ground-vegetation surface. Soil-layer temperature is resolved with a Crank-Nicholson numerical scheme. Diffusion equations for the soil temperature determine ground heat flux. The Noah LSM uses soil and vegetation lookup tables for static soil and vegetation parameters such as porosity, hydraulic conductivity, minimum canopy resistance, roughness length, leaf area index, etc.

2.1.2. Noah augmented with a short-term dynamic phenology module (DV)

We coupled the canopy module of Dickinson et al. (1998) to STD in order to compute changes in vegetation greenness fraction that result from environmental pertubations. The module allocates carbon assimilated during photosynthesis to leaves, roots, and stems; the fraction of photosynthate allocated to each reservoir is a function of, among other things, the existing biomass density. The model also tracks growth and maintenance respiration and represents carbon storage. Unlike STD, which computes greenness fraction by linear interpolation between monthly climatological values, DV represents short-term phenological variation by allowing leaf area to vary as a function of soil moisture, soil temperature, canopy temperature, and vegetation type. DV makes vegetation fraction an exponential function of leaf area index (LAI) (Yang and Niu, 2003). Because DV links vegetation fraction to dynamic LAI, DV makes direct soil evaporation, canopy evaporation, and transpiration more responsive to environmental conditions than STD. Unlike Dickinson et al. (1998), we parameterize the effect of water stress on stomatal conductance as a function of soil moisture deficit, not as a function of soil matric potential.

2.1.3. Noah augmented with a simple groundwater model (GW)

GW couples a lumped unconfined aquifer model (Niu et al., 2007) to the lower boundary of the STD soil column. In GW, water flows vertically in both directions between the aquifer and the soil column. The modeled hydraulic potential is the sum of the soil matric and gravitational potentials. The relative water head between the bottom soil layer and the water table determines either gravitational drainage or upward diffusion of water driven by capillary forces. Aquifer specific yield is used to convert the water stored in the aquifer to water table depth. When water is plentiful, the water table is within the model's soil column; if water is insufficient to maintain a near-surface aquifer, the water table falls below the soil column. An exponential function of water table depth modifies the maximum rate of subsurface runoff (for computation of baseflow) and determines the fraction of the grid cell that is saturated at the land surface (for calculation of surface runoff) (Niu et al., 2005). The model does not explicitly consider lateral transport of groundwater between grid cells.

2.2. IHOP_2002 sites and datasets

We used datasets available at http://www.rap.ucar.edu/research/land/observations/ihop/ from the IHOP_2002 field campaign (Weckwerth et al. 2004; LeMone et al., 2007) to evaluate the three versions of Noah LSM at nine sites along the Kansas-Oklahoma border and in northern Texas (Fig. 1). The nine stations were sited to obtain a representative sample of the region, which spans a strong east–west rainfall gradient and Bowen ratio. We used 45 days of high-frequency, multi-sensor measurements of meteorological forcing, surface-to-atmosphere fluxes, and near-surface soil moisture and temperature. Site characteristics, soil and vegetation classes, mean meteorological values, average heat fluxes and near-surface states for the observation period are summarized in Table 1.

2.3. Model initialization and spin-up

Following Rodell et al. (2005), we initialized each of the four soil layers at 50% saturation and at the multi-annual-mean temperature. To drive the spin-up (between January 1, 2000, and May 13, 2002), we used downscaled North American Land Data Assimilation System (NLDAS) (Cosgrove et al., 2003) meteorological forcing, interpolated from a 60-minute to a 30-minute time step. The models were subsequently driven by IHOP_2002 meteorological forcing from May 13, 2002, to June 25, 2002 (DOY 130 to 176). For GW, water table depth was initialized assuming equilibrium of gravitational and capillary forces in the soil profile (Niu et al., 2007).

2.4. Evaluation datasets

To constrain and evaluate the models, we used sensible heat flux (H), latent heat flux (LE), ground heat flux (G), ground temperature (Tg), and first layer soil moisture (SMC_{5cm}). All data was recorded at a 30-minute time step. In situ, high-frequency flux and near-surface state measurements are an integrated response of the land surface and therefore provide useful data for examining model soundness at a specific location (Bastidas et al., 2001; Stockli et al., 2008). To score model performance, we used root mean square error (RMSE).

2.5. Parameters considered in the sensitivity analysis

We selected 10 soil and 10 vegetation parameters of STD that have been deemed important at similar locations (Demarty et al. 2004; Bastidas et al., 2006). We included eight parameters responsible for the phenology module and four that control the groundwater module to analyze a total of 28 and 24 parameters for DV and GW, respectively. All other coefficients in the models were kept constant at the recommended values. Default values and feasible ranges (Table 2) for all parameters were taken from the literature (e.g., Chen and Dudhia, 2001; Hogue et al., 2006).

2.6. Methods for sensitivity analysis

We use the variance-based method of Sobol' (Sobol', 1993; 2001) to efficiently identify the factors that contribute most to the variance of a model's response. Unlike RSA, the method of Sobol' deals explicitly with parameter interaction and has recently been used to quantify model sensitivity and parameter interactions in hydrology (e.g., Ratto et al., 2007; Tang et al., 2006, 2007; Yatheendradas et al., 2008; van Werkhoven et al., 2008). To our knowledge, it has not yet been used for LSM SA.

Since variance-based SA (VSA) does not allow a mapping of the sensitivity back to the parameter space, we complemented our evaluation with regionalized sensitivity analysis (RSA).

2.6.1. Sobol' indices for global variance-based sensitivity analysis (VSA)

Sobol' indices enable researchers to distinguish the subset of independent input factors X={x_1, .,x_i,., x_k}that account for most of the variance of the model's response $Y=f(X)$ either by themselves (first-order) or due to interaction with other parameters (higher-order). For completeness, here we summarize the efficient Monte Carlo-based scheme presented by Saltelli (2002) to compute first-order and total Sobol' sensitivity indices.

The first-order sensitivity index (S_i) represents a measure of the sensitivity of $Y = f(x_1, x_2, ..., x_k)$ (the RMSE of a model realization evaluated against observations) to variations in parameter x_i. S_i is defined as the ratio of the variance of Y conditioned on the i^{th} factor (V_i) to the total unconditional variance (V):

$$S_i = \frac{V_i}{V(Y)} = \frac{V(E(Y \mid x_i))}{V(Y)} = \frac{\hat{U}_i - \hat{E}^2(Y)}{\hat{V}(Y)} \qquad (1)$$

Where $$\hat{U}_i = \frac{1}{n-1}\sum_{r=1}^{n} f(x_{r1}, x_{r2}, ..., x_{rk}) f(x'_{r1}, x'_{r2}, ..., x'_{r(i-1)}, x_{ri}, x'_{r(i+1)}, ..., x'_{rk}) \qquad (2)$$

is obtained from products of values of f computed from the sample matrix (n model realizations long) times values of f computed from another n-realizations matrix where all k parameters except x_i are re-sampled.

The estimates of the mean squared and the total variance are computed as:

$$\hat{E}^2(Y) = \frac{1}{n}\sum_{r=1}^{n} f(x_{r1}, x_{r2}, ..., x_{rk}) f(x'_{r1}, x'_{r2}, ..., x'_{rk}) \tag{3}$$

$$\hat{V}(Y) = \frac{1}{n}\sum_{r=1}^{n} f(x_{r1}, x_{r2}, ..., x_{rk})^2 - \hat{E}^2(Y) \tag{4}$$

Instead of computing all 2^k-1 terms of the variance decomposition:

$$V(Y) = \sum_{i}^{k} V_i + \sum_{i}\sum_{j>i} V_{ij} + ... + V_{12..k} \tag{5}$$

(which would require as many as $n2^k$ model runs), in addition to estimating S_i, it is customary to estimate only the total sensitivity index (S_{Ti}) associated with parameter x_i. S_{Ti} encompasses the effect that of all the terms in the variance decomposition that include the factor x_i have on the variance of the model's response. S_{Ti} is estimated by the difference between the global unconditional variance of Y and the total contribution to the variance of Y that is caused by factors other than x_i, divided by the unconditional variance:

$$S_{Ti} = \frac{V(Y) - V(E(Y|x_{-i}))}{V(Y)} = 1 - \frac{\hat{U}_{-i} - \hat{E}^2(Y)}{V(Y)} \tag{6}$$

Where
$$\hat{U}_{-i} = \frac{1}{n-1}\sum_{r=1}^{n} f(x_{r1}, x_{r2}, ..., x_{rk}) f(x_{r1}, x_{r2}, ... x_{r(i-1)}, x'_{ri}, x_{r(i+1)}, ... x_{rk}) \tag{7}$$

is obtained from products of values of f computed from the sample matrix times the values of f computed from another matrix where only x_i is re-sampled. To spare nk simulations for each model and each site (and to show that is possible to mine regular Monte Carlo runs, customary used in land-surface modelling), we estimated the second part of this term by interpolating the response surface Y (as explained in Section 2.7.3).

A significant difference between S_{Ti} and S_i points to an important role of the interactions of the i^{th} factor (at all orders) in affecting Y (Saltelli et al., 2006). Identification of such parameter interactions can help guide model development. S_{Ti} are also useful to identify input factors that are non-influential, which can help reduce the dimensionality of the parameter estimation problem. If an S_{Ti} is negligible, then it is reasonable to fix that factor to any value within its range of uncertainty, and the dimensionality of the space of input factors or model parameters can be reduced accordingly (van Werkhoven et al., 2009).

2.6.2. Kolmogorov-Smirnov test for regionalized sensitivity analysis (RSA)

In RSA (Hornberger and Spear, 1981; Spear et al., 1994; Bastidas et al., 1999, 2006), the Kolmogorov-Smirnov (K-S) test helps identify which parameters differ when model performance is 'behavioral' (B) ('good', 'acceptable') versus 'non-behavioral' ($\bar{B}$). Note that RSA does not give any information regarding the extent to which a parameter affects the variance of the model output. It instead focuses on which factors are believed to affect the occurrence of behavioral model realizations.

The two-sample K-S test (two-sided version) is independently applied to the univariate marginal cumulative density functions (CDF) of each parameter to test whether the distributions of B and $\bar{B}$ are different at a particular significance level. The maximum distance between the two CDFs serves to evaluate the null hypothesis that the parameter values come from the same probability distribution. It is intuitive that, if the CDFs are dissimilar from one another (as well as different from the a priori marginal distribution of that parameter), then such parameter is 'sensitive' (Saltelli, 2006).

Generally, a set of subjective constraints or thresholds provides a qualitative definition for B, and model realizations are classified into either B or $\bar{B}$. In the research presented here, we considered the calibrated parameter sets (which belong to the joint posterior probability distribution that maximizes the likelihood function) as representative of B. The $\bar{B}$ sample was defined by parameter sets whose RMSE is half a standard deviation or more away from the mode of the cost function. For robustness, for each parameter, several different samples from $\bar{B}$ were taken and compared to the one of B. We used 5% as the significance level for our RSA.

2.7 Sampling strategies for sensitivity analysis

We generated representative samples of model parameters using Latin Hypercube Sampling (LHS) and of the behavioral parameter sets through multi-objective calibration. We also sampled from the response surfaces obtained via LHS using inexpensive Support Vector Machines (SVM).

2.7.1 Latin Hypercube Monte Carlo sampling (LHS)

We ran a total of 405,000 Monte Carlo simulations sampling random parameter sets (15,000 samples for each model and site) to obtain a detailed representation of the range of model responses. We used LHS because it combines the strengths of stratified and random sampling to ensure that all regions of the parameter space are represented in the sample (McKay et al., 1979; Helton and Davis, 2003). LHS divides each parameter range into disjoint intervals of equal probability. From each hypercube, one sample value is randomly taken. We sampled uniformly within feasible bounds (Table 2). For each sample, we recorded the RMSE of 5 criteria: H, LE, G, Tg, and SMC_{5cm}.To create all the matrices involved in the computation of the S_i index of the Sobol' method (Eq. 1), we used a modified LHS that enables replication. We sequentially sampled the same parameter value twice from a given hypercube, while all other parameters in the set were chosen according to the LHS.

2.7.2 Multi-objective Markov Chain Monte Carlo parameter estimation technique

We used the efficient Markov Chain Monte Carlo sampling strategy of Vrugt et al. (2003) to approximate the joint posterior distribution of optimal parameters. The simultaneous minimization of the RMSE of multiple criteria {H, LE, G, Tg, SMC_{5cm}} allowed us to constrain the models to be consistent with several types of observations and facilitated the identification of the underlying posterior distribution of physically meaningful behavioral parameter sets. It is hoped that sets from the posterior distribution cause the model to mimic the processes it was designed to represent (Gupta et al., 1999; Bastidas et al., 2001; Leplastrier et al., 2002; Hogue et al., 2006). The calibration algorithm runs, in parallel, multiple chains of evolving parameter distributions to provide a robust exploration of the parameter space. These chains communicate with each other through an external population of points, which are used to continuously update the size and shape of the proposal distribution in each chain. This procedure allows an initial population of parameter sets (uniformly sampled within pre-established, feasible ranges) to converge to a stationary sample, which maximizes the likelihood function and fairly approximates the Pareto set. The Pareto set (PS) represents the multi-objective tradeoff: no member of the PS can perform better with respect to one objective without simultaneously performing worse with respect to another competing objective (Gupta et al., 1998). We used a sample of 150 parameter sets to represent the posterior distribution of 'behavioral' parameter sets (*B*).

2.7.3 Response surface sampling (meta-modeling) using Support Vector Machines (SVM)

To inexpensively compute the second component of the U_{-i} term (Eq. 7) for the Sobol' method (Section 2.6.1), we approximated the response surfaces of the LSMs using SVM trained on the Monte Carlo samples. We used the SVMlight libraries of Joachims (1999) available at http://svmlight.joachims.org/.

SVM are a robust learning strategy that efficiently generalizes a non-linear functional dependence between a set of multi-dimensional inputs and a vector of outputs, $Y=f(X)$. SVM use kernels to map the complex data into high-dimensional feature spaces in which linear relationships can describe separation planes. Through a sparse set of training examples that 'support' the hyperplane that best fits the observed data, SVM create a model to approximate Y (Vapnik, 1998). SVM have been successfully applied in a variety of hydrological applications (e.g., Asefa et al., 2004, 2005, 2006; Khalil et al., 2005; Kaheil et al., 2008a, 2008b). SVM perform better than artificial neural networks (Dibike et al., 2001; Gill et al., 2008), with lower complexity (only 3 parameters), less computational cost (faster training), and reduced sensitivity to noisy inputs and sparse training samples.

Based on statistical learning theory (Smola and Schölkopf, 2004), SVM are characterized by a mechanism that avoids overfitting and that results in good generalization. A coefficient C determines the tradeoff between the complexity (or flatness) of the function f and the amount to which deviations larger than empirical error ε are tolerated. In the SVM training, prediction error and model complexity are simultaneously minimized in a quadratic optimization problem, which results in a uniquely global optimum (Vapnik, 1998). We used Gaussian radial basis function kernels and determined near-optimal values of the 3 SVM hyper-parameters (the capacity C, the soft margin ε and the kernel width γ) using the SCE calibration algorithm (Duan et al., 1992).

For detailed explanation on the estimation procedure for SVM parameters, we refer interested readers to Khalil et al. (2006).

The error in the estimation of the U_{-i} term is small. For example, an SVM (C=97.12, ε= 0.0025 and γ= 0.0323) trained on 5,000 random samples of GW [Y= RMSE(SMC_{5cm})] at Site 9 (and calibrated against other 5,000 testing samples) predicted the remaining independent validation samples from the Y surface with a RMSE of 0.93 [%]. The estimated variance of Y (8.857) is only 3% different than the 'true' variance (8.584) obtained by the Monte Carlo runs.

2.8. Hierarchical clustering for comparisons of parameter distributions

Unsupervised classification of behavioral parameter distributions allowed us to gain understanding about the similarities of the data across locations, specifically about the relationships between types of parameters and sites. We used clustering methods to separate the collection of marginal posterior distributions of calibrated parameters sets into groups. Agglomerative hierarchical clustering methods start with n groups (one object per group) and successively merge the two most similar groups until a single group is left. We used MATLAB's complete linkage algorithm, in which the maximum distance between objects, one coming from each cluster, represents the smallest sphere that can enclose all objects in the two groups into a single cluster (Hair et al., 1995). Since the distance used to measure dissimilarity between observations (e.g., Manhattan, Euclidean, etc.) may influence the membership of samples to groups, we used the cophenetic correlation coefficient to assess the quality of the linkage (Martinez and Martinez, 2002). We used dendrograms to show the links between the objects as inverted U-shaped lines, whose height represents the distance between the objects.

3. Driving questions and experimental design

We first ask: What are the dominant model parameters across the region? We ran a suite of Monte Carlo simulations to identify parameters that exert the greatest control on the variability of simulated fluxes and states at each IHOP site for all 3 models (STD, GW and DV). We quantify sensitivity using RSA and the method of Sobol'. Our SA guides our further investigation.

We then address the question: What are the dominant interactions between model parameters, and how do these change between models? With our focus toward model development, we investigate the relationships between behavioral model parameters and quantify how they change between models using the estimates of the total-order sensitivity, the multivariate posterior parameter distributions, and the covariance structures.

We finally ask: How do behavioral parameters change with dominant physical characteristics of the land? We summarize the relationships between model parameters and physical characteristics by classifying the multivariate posterior distributions according to types of soil and vegetation. Our classification provides insights into how parameters can be transferred to ungauged locations.

4. What parameters are sensitive?

We report the results of our regionalized and variance-based sensitivity analyses, which we use in the next section to help evaluate model behavior.

4.1. Regionalized sensitivity analysis (RSA)

The sensitivity of a given parameter changes between models and varies by location, without an easily recognizable pattern. Table 3 presents the model parameters deemed sensitive at the 5% significance level according to a Kolmogorov-Smirnov (K-S) test between samples that drive behavioral (multi-objectively calibrated) and non-behavioral simulations. A value of 1 means the parameter is sensitive, 0 means insensitive. The number of sensitive parameters is tabulated by site and by class. In all versions of Noah LSM, soil parameters tend to be more sensitive than vegetation parameters.

At five of the nine sites, GW has the fewest number of sensitive parameters of any of the three models, despite having more total parameters than STD. At the dry sites (1-3), the addition of GW reduces the number of vegetation parameters that are sensitive, perhaps because when GW processes are not included, the vegetation parameters are given more weight in controlling the water balance of the soil. At site 9, despite decreasing the number of sensitive vegetation and soil parameters with respect to STD, GW does not even make the parameters associated with GW sensitive.

DV most often has the highest number of sensitive parameters. The number of vegetation parameters at dry sites that are sensitive in DV is significantly higher than at wet sites. Not surprisingly, the conversion factor (*gl*) and the specific leaf area (*sla*) are sensitive everywhere. The fraction of carbon into growth (*fragr*) and the water stress parameter (*wtsr*) are sensitive at eight sites, while the coefficient for soil respiration (*rssoil*), the optical depth (*tauhf*) and the wood allocation parameter (*bf*) are the least often sensitive. The variability of parameter sensitivity between even similar sites perhaps points to a lack of constraint of DV with respect to the partitioning of the carbon budget or suggests that interactions with other parameters decreases the separation of the CDFs, consequently hindering the identification of sensitive parameters (Yatheendradas et al., 2008).

The widespread use of RSA in LSM development has been precluded by what has been RSA's lack of firm conclusions because of the relatively poor agreement between the conclusions of RSA studies. Even though we and Bastidas et al. (2006) used roughly the same version of Noah (STD) and allowed many of the same parameters to vary, we found that our RSA is at best partially consistent with the assessment of Bastidas et al. (2006). One possible reason for our divergent assessments is that we did not analyze exactly the same parameters and did not sample from exactly the same ranges as did Bastidas et al. A single parameter's sensitivity, as defined in RSA approaches, is likely a function of the values of other model parameters; alteration of the sampled range of a single parameter can influence the sensitivity of many other parameters (Spear and Hornberger, 1980). Results presented elsewhere (Rosero et al., 2009) have shown that adjusting only a partial set of parameters alters model structure (i.e., the relationships between parameters); it follows that, with changed model structure, regionalized sensitivity would also vary.

Perhaps the most important reason why information obtained through RSA has not been used to inform LSM development is that RSA provides neither information regarding the magnitude of a parameter's influence on model output nor information about the influence that the parameter exerts through interactions. RSA only identifies a subset of parameter sets that improves (if only slightly) model output. A K-S statistic that corresponds to 'high sensitivity' means the parameters used to generate the behavioral model realizations are 'a lot different' from those used to generate the nonbehavioral realizations. 'High sensitivity' does not mean that a parameter is highly important to (exerts significant control over) model output. Furthermore, having invariant parameter distributions in the transition from $\bar{B}$ to B is a necessary but not sufficient condition for insensitivity (Spear and Hornberger, 1980). Quantifying regionalized sensitivity has the potential to allow a mapping of the model sensitivity to parameters back to the parameter space, but without information on the change in model's variance, RSA appears only useful for limiting the dimensionality of the calibration problem at a specific site.

RSA is distinct from the variance-based analysis of sensitivity in model output to parameter values. The method of Sobol' identifies parameters that exert significant control on the variance of model output. Sobol' indices are arguably a more useful tool for model developers and the model's operational users.

4.2 Global variance-based sensitivity analysis (VSA)

Our VSA shows that there are only a few parameters that, by themselves, exert significant influence on model predictions. In contrast, parameter interaction predominates and is hence the principal mechanism for sensitivity. Figures 2, 3, and 4 present, for all sites, all considered parameters, and all models, the Sobol' first-order sensitivity indexes (S_i, which is the fraction of the total variance of RMSE that can be solely attributed to the i^{th} parameter) and the residual between Sobol''s total and first-order sensitivity index ($S_{Ti} - S_i$, which is the fraction of total variance that results from the interaction of the i^{th} parameter with other parameters at all orders). The easily recognizable pattern of sensitivity can be linked to physical characteristics of the sites.

4.2.1 First-order sensitivity (S_i)

The identified sensitive parameters (Figs. 2-4) are consistent with our expectations. When parameter influences changes as we would physically expect, we interpret these results as consistent with our hypothesis that to a first order, the models are adequately representing the site-to-site variation in these key components of the water and energy cycles. We observe that, for most sites and models, the greatest first-order control on simulated top-layer soil moisture is porosity (*maxsmc*) (Fig.4a). At dry sites 1-3, where direct evaporation is presumably a major component of LE flux, for STD and GW, the bare soil evaporation exponent (*fxexp*) exerts the most first-order control on soil moisture. The LE flux simulated by GW at dry sites is controlled by *fxexp* and specific yield (*rous*), which controls depth to the water table. *lai* directly exerts control on transpiration and hence on the surface energy budget; at the most vegetated sites (7-9), *lai* consequently shapes the most the variance of H and LE for both STD and GW (Fig 2a, 3a). The initial value *lai* is not important to determining DV's simulated H and LE because, unlike the other two models, DV allows the initial value of *lai* to change. Instead, minimum stomatal resistance (*rcmin*) exerts the most control on DV-simulated LE flux. Two new parameters associated with DV, *gl* and *sla*, which control the calculation of *lai*, also exert first-order control on the simulated energy balance. In sparsely vegetated sites (1-3), the Zilintikevich coefficient (*czil*) plays a significant role in the variance of H.

The control of parameters on model variance changes between models and between sites. The shift in dominant parameters gives clues about how the models are representing the water and energy cycles from semi-arid (1-3) to semi-humid (7-9) sites. Looking only at STD, we see that as the mean annual precipitation (MAP) at the sites increases, *fxexp* becomes less important to determining the top-layer soil moisture, and *refkdt*, a parameter involved in determining maximum rates of infiltration, becomes more important (Fig. 4a). Expanding our view to include GW, in which surface runoff is de-emphasized and subsurface runoff is emphasized (see discussion about GW's preferred modes of operation, Section 5), we see that although *fxexp* is still a key parameter exerting first-order control on SMC at the dry sites, *refkdt* has little direct influence on soil moisture at the wet sites. The most sensitive parameter for SMC_{5cm} at sites 1-3 is the aquifer's specific yield (*rous*), which effectively controls whether aquifer water will be accessible to the near-surface soil. Consistent with our expectations, soil suction (*psisat*), which in GW controls upward movement of water from the aquifer to the soil, has significant control on SMC within GW but not within STD, in which *psisat* exerts less control over soil hydraulic behavior (Fig. 4a).

As sites get progressively wetter, surface exchange coefficient *czil* exerts progressively less influence on simulated H, and *rcmin* exerts progressively more influence on H (Fig. 2a). The shift in control is consistent with our expectation that at more vegetated sites, stomatal resistance will be more important to determining the surface energy balance. As a site's MAP increases, *rcmin* and *lai* have increasing control over simulated LE, while *fxexp* becomes less influential (Fig. 3a). Even at dry sites (1-3), DV tends to favor larger values of vegetation fraction (*shdfac*) than are prescribed by STD and GW. As a consequence, DV stands apart from GW and STD in that *fxexp* does not directly contribute to variance of any objective at the three driest sites (with the exception of the unvegetated, bare-soil site 1, where LE is controlled by *fxexp*).

Examinations of S_i that are not in line with expectations may be used to help modelers diagnose problems with forcing data and/or model structure. For instance, *fxexp* has the highest S_i of simulated H and LE at site 6. Site 6 receives 800 mm of precipitation each year. We do not expect direct evaporation to be a more significant component of the LE flux at site 6 than at climatically simliar sites 4 and 5 or at the semi-arid sites 1-3. The discrepancy implies that our conceptual understanding of the physical processes at site 6 is incorrect, that the model does not adequately represent the physical processes, and/or that our forcing and/or evaluation data are faulty.

In contrast to what was observed with RSA, the VSA shows a clear pattern of sensitivity across the sites. Site-to-site variation in the most sensitive parameters is not chiefly governed by soil or vegetation type but, similar to other studies (e.g, Liang and Guo, 2003; Demaria et al.

2007; van Werkhoven et al., 2008), appears to be of secondary importance when compared to the influence of climatic gradient.

4.2.2 Sensitivity through interactions (S_i–S_{Ti})

Figures 2b, 3b, and 4b show that interactions between parameters are responsible for most of the variance in the models' predicted H, LE, and SMC. If we assume that the parameterizations are correct, then the significant parameter interaction indicates model overparameterization (Saltelli et al., 2008). Overparameterization causes increased parameter interaction (observed here) and decreases the percentage of parameters that are deemed sensitive by RSA (Bastidas et al., 2006; Yatheendradas et al., 2008) (observed in the RSA described above). VSA enables the quantification of the significance of parameter interaction and the identification of the most interactive parameters. Although parameter interaction may not be an inherently negative trait (e.g., in porous media, we expect hydraulic conductivity and porosity to be functionally related), especially when there are no known functional relationships between the physical quantities that developers believe two parameters represent, parameter interaction is likely to be indication that the model is working in ways that are not consistent with the conceptual model from which the parameterizations were built.

All models exhibit the most parameter interaction at the driest sites, consistent with the findings of Liang and Guo (2003) and suggesting the need to revise the formulation of all three models for semi-arid regions (Hogue et al., 2005; Rosero and Bastidas, 2007). Especially for H and SMC, GW reduces parameter interaction at the middling moisture (4-6) and semi-humid sites (7-9) (e.g., Fig.5b). GW's reduction of parameter interaction is evidence (although by no means conclusive) that GW is more realistic than STD at sites 4-9. This is consistent with observations on the robustness of GW (Gulden et al., 2007). Conversely, GW appears to produce significant parameter interaction at semiarid sites 1-3, indicating a need for an improved parameterization of groundwater processes at semi-arid sites. DV parameters are much more interactive than those of STD and GW, especially at the wettest sites when simulating LE and SMC. The increased interaction between the DV-specific parameters and the rest of the conceptually unrelated STD parameters suggests DV is not functioning as its developers intended. The significant parameter interaction is consistent with the poor robustness of DV (Rosero et al., 2009).

There is significant interaction between the vegetation parameters and the sensitivity of soil parameters. These results fully support the findings of Demaria et al. (2007) and Liang and Guo (2003). The significant interplay between soil and vegetation parameters implies that parameter interaction between different model parts changes both the optimal value of a given parameter and the relationships between parameters. In the next section, we use the multivariate posterior distribution of behavioral parameters to characterize the impact of adding new modules on parameter interactions.

Looked at in full, we conclude that the models best represent the surface water and energy balance at the intermediate moisture and wet sites, where parameter interaction tends, within a given model, to be lowest. Because it reduces parameter interaction, GW is most likely of any of the three models to be representing the key physical processes with the most realism.

5. How do sensitive parameters interact and shape model behavior?

We present a case study in which sensitivity analysis (SA) links model identification and model development. SA identifies parameters whose behavior merits further examination: VSA indicates which parameters are most influential in determining model output; RSA helps us identify modes in parameter distributions that yield distinctive model behavior.

5.1 A case study at Site 7

At site 7, STD, DV, and GW show nearly equivalent performance when using their behavioral parameter sets (Figs. 5, 6). Such 'equifinality' is well documented in the hydrologic modeling literature (e.g. Beven and Freer, 2001; Rosero et al., 2009). In this case, distinguishing a 'best' model is not trivial. It requires us not only to confront the simulations with observed behavior to test for consistency but to fully understand the underlying model structures (the relationship between parameters) that make STD, GW and DV perform equally well. We show how sensitivity analysis offers the power and the ability to discriminate between model structures that conform to our physical understanding of the systems.

5.2 Focus on sensitive parameters to better understand model function

We follow the impact of shifted preferred values of three 'physically meaningful' parameters that made considerable contributions to first-order variance: porosity (*smcmax*), the muting factor for vegetation's effect on thermal conductivity (*sbeta*), and minimum stomatal resistance (*rcmin*). The fundamental implication of our observations is that although the different optimal values of parameters are important (as found during model identification), the change in functional relationship between the parameters (the information contained in the interactions) is most relevant for purposes of model development.

Figure 7 shows the marginal CDF of the posterior multivariate distribution for selected sensitive parameters in the behavioral range at Site 7. Along with the CDFs, box plots show the median and interquartile ranges of the skewed parameter distributions. The scatterplots show the variation in RMSE of LE and SMC_{5cm} along the range of plausible values of the parameter. The trend is emphasized by fitting the points with a polynomial of minimal complexity. Even a cursory analysis of Figure 7 shows that the direction of 'sensitivity' (understood as the rate of change of score with parameter value) changes between models (e.g., Fig. 7a). The simulation of SMC_{5cm} by STD and DV degrades as porosity increases, while GW improves. We also note that, along the plausible range, the response can be enhanced (Fig. 7d) or become relatively insensitive to changes in parameter value (Fig. 7c). The identifiability of parameters (understood as having a clearly defined local minimum) changes between models. For example, in DV, there is a clear low point of the RMSE of LE along the range of values of the maximum water-holding capacity of the canopy (*cmcmax*), but STD and GW have less of a preference (Fig. 7c). The interquartile range of *rcmin* of STD is smaller than that of GW or DV (Fig. 7b). We can clearly see that different models have distinct optimal parameter values for the same physical parameter, implying not only that the parameters cannot be transferred between models but that the relationships between them are different.

5.2.1 The role of porosity (*maxsmc*)

In all three versions of Noah, higher values of *maxsmc* tend to decrease direct evaporation from the first soil layer (E_{DIR}). E_{DIR} is estimated as the product of Penman's potential evaporation (ET_{pot}), the complement of the vegetated fraction (*shdfac*), and the ratio of top-layer volumetric soil moisture (SMC_1) to *maxsmc*:

$$E_{DIR} = ET_{pot}(1 - shdfac)\left(\frac{SMC_1 - SMC_{dry}}{maxsmc - SMC_{dry}}\right)^{fx\exp} \tag{8}$$

SMC_{dry} is the lowest volumetric water content that can exist in the top soil layer, and *fxexp* is a parameter ranging from 0.2 to 4.

In STD and DV, the error in simulating LE tends to be relatively small when *maxsmc* is low and relatively large when *maxsmc* is high (Fig. 7a). However, GW shows slight improvement in simulating LE as *maxsmc* increases. The tendency of STD and DV to simulate LE well when *maxsmc* is low (and direct evaporation from the soil consequently tends to be high) implies that STD and DV often underestimate direct evaporation at site 7. Given the same *maxsmc* value, GW more easily simulates sufficient direct evaporation, perhaps because of wetter soil (Rosero et al., 2009).

In STD and DV, *maxsmc* controls both surface and subsurface runoff. Hydraulic conductivity of the soil layer (*wcnd*) is computed using Clapp and Hornberger's method, which scales saturated hydraulic conductivity (*dksat*) by wetness (SMC/ *maxsmc*), raised to an exponent determined by the Clapp and Hornberger parameter (*b*):

$$wcnd = dksat\left(\frac{SMC}{maxsmc}\right)^{2b+3} \tag{9}$$

Lower *maxsmc* yields higher *wcnd*, which means water moves through the soil more quickly. Note that, in the case of parameterizing subsurface runoff, hydraulic conductivity is a representation of the speed at which the water can move laterally through the soil. In STD and DV, subsurface runoff (*Runoff2*) is *wcnd* times the slope. Consequently, higher values of *maxsmc* decrease *Runoff2*. Higher values of *maxsmc* also decrease surface runoff (*Runoff1*) by increasing the maximum rate of infiltration. Both changes increase the wetness of the surface soil.

GW changes the way runoff is computed; *maxsmc* does not control surface or subsurface runoff in GW, eliminating two of the three ways in which *maxsmc* controls soil moisture. *Runoff2* is represented as an exponential function of depth to water (Niu et al., 2007):

$$Runoff2 = rsbmx\, e^{-fff^{*}z_{WT}} \tag{10}$$

Where *rsbmx* is the maximum rate of subsurface runoff, *fff* is the e-folding depth of saturated hydraulic conductivity, and Z_{WT} is a variable that represents the depth to the water table. *Runoff1* is a modified version of the same function used to compute subsurface runoff (Niu et al., 2005):

$$Runoff1 = pcpdrp*\left(fsatmx\, e^{-0.5*fff*Z_{WT}}\right) \quad (11)$$

Where *pcpdrp* is the effective incident water and the second term is the fraction of unfrozen grid cell that is saturated.

In STD (and DV), *maxsmc* couples two physically unrelated (or very weakly related) processes (direct soil evaporation and lateral surface and subsurface runoff). GW decouples these processes by eliminating the dependence of parameterized lateral runoff on *maxsmc*. This decoupling reduces the spurious parameter interaction of *maxsmc* and, within GW, virtually eliminates the tradeoff between good simulation of LE and SMC5cm. GW is, in this regard, a better model for simulating fluxes at site 7.

The question remains – why does GW poorly simulate SMC when *maxsmc* increases? *maxsmc* is used to compute vertical hydraulic conductivity (using the same function described above), which GW uses to control the flow of water between the aquifer and soil down a hydraulic gradient. Higher *maxsmc* yields lower hydraulic conductivity, which, in addition to decreasing the transfer of water between layers within the soil column, decreases the communication between the aquifer and the soil profile (that is, it decreases the flow of water between the two, increasing the potential for water to be retained near the surface). At site 7, GW best simulates SMC when high vertical hydraulic conductivity connects the aquifer and soil.

Consistent with the work of others (e.g., Demaria et al., 2007), parameter values and model sensitivity to *maxsmc* are not consistent between sites along a climatic gradient or even within a set of sites with similar characteristics. Conclusions about model performance are therefore difficult to generalize. This lack of continuity of behavior between sites is consistent with at least one of the following possibilities: (1) model parameterizations do not represent key aspects of the system and/or (2) our multi-objective calibration provided insufficient constraint for the estimation of behavioral parameters. We recommend use of runoff constraints before drawing firm conclusions regarding the physical reality of the runoff-related processes in GW.

5.2.2 The role of SBETA

All three models compute ground heat flux (G) using a flux-gradient relationship:

$$G = DF_1 \frac{STC_1 - T_1}{0.5 * ZSOIL_{(1)}} \tag{12}$$

In which STC_1 is the temperature at the center of the first soil layer ($0.5*ZSOIL_{(1)}$) and T_1 is the surface temperature. DF_1 is the heat conductivity of the top soil layer.

Noah assumes that, as vegetation cover increases, heat flux into the ground decreases. It uses parameter *sbeta* and the vegetated fraction (*shdfac*) to mute the thermal conductivity of the top layer of the soil (DF_1) by:

$$DF_1 = DF_1 * e^{sbeta * shdfac} \tag{13}$$

At site 7, the mode of the posterior probability distribution of all three models is near the bound of the explored parameter range (-1) (Fig. 7d). The preference for near-bound values is more pronounced in DV, which at site 7 tends to have *shdfac* values near 1.0, which puts downward pressure on the value of *sbeta*. The skewed posterior parameter distribution for all suggests that an even-less-negative value of *sbeta* would have yielded better results at site 7.

The assumption that vegetation necessarily decreases the thermal conductivity of the top layer of the soil may be incorrect. If the 'vegetation effect' on thermal conductivity is real, the model underestimates the top-layer soil thermal conductivity. At site 7 (and at several other sites), there is a clear tradeoff between H and G that is mediated by the thermal conductivity which hints at the need for revised process understanding.

When comparing site 7 simulations to those of the other two 'wet' sites (8 and 9), we see a roughly consistent preference for near-zero values of *sbeta*. At the drier sites (1-6), the model's strong preference for near-zero values of *sbeta* is less obvious; however, *shdfac* is closer to zero at these sites, which lowers the value of the muting factor described by Eq.13.

5.2.3 The role of minimum stomatal resistance (*rcmin*)

rcmin controls much of the variance in H and LE, especially at wetter sites. As *rcmin* increases, the ratio of actual to potential evapotranspiration decreases. *rcmin* has a more consistent influence on the variance of H than on LE.

At site 7, all three models prefer a low *rcmin* (Fig. 7b), which increases LE for a given potential evapotranspiration; however, GW and DV show decreased identifiability of *rcmin*. The mode of the *rcmin* distribution is higher for GW than for STD, perhaps because GW tends to have a wetter soil and more robust LE. The spread of the posterior distribution of *rcmin* for DV is significantly larger than that for STD, although both models share the same mode. This decrease in identifiability of parameters functionally related to *lai* (as is *rcmin*) is consistent with the added degrees of freedom allowed by DV (DV parameters *gl* and *sla* are most important in predicting *lai* [Fig. 2]). Because DV simulations include a wider spread of *lai* states, they also have a wider spread of 'good' *rcmin* values.

5.3 What changes in GW to make it work better than or as well as STD at Site 7?

Figure 8 shows the bivariate posterior distribution of selected behavioral parameters of STD and GW. The response surface of RMSE SMC_{5cm} changes between STD and GW (e.g., see *maxsmc* vs. *psisat*). For GW, the shape of the posterior distributions of soil parameters that are shared with STD is significantly different because of interaction with the GW parameters and module. Such shifts in model function affect the model covariance structure (Table 4).

After multi-objective parameter estimation, at site 7, GW functions in one of two preferred modes (Fig. 8b). In the first, slightly preferred mode (*m1*), the parameters work together to help GW function as the developers likely intended. Strong communication between the aquifer and the soil column is supported by relatively high values of saturated hydraulic conductivity (*satdk*), low values of the reciprocal of the e-folding depth of hydraulic conductivity (*fff*), and low porosity (*maxsmc*). A relatively low surface runoff scaling factor (*fsatmx*) and relatively high subsurface runoff scaling factor (*rsbmx*) ensure that subsurface runoff dominates surface runoff. Mimicking nature, high soil suction (*psisat*) pulls water upward. A high aquifer specific yield (*rous*) deepens the water table (weakening the direct influence of the saturated zone on the model soil column) and transforms more water to runoff rather than to recharge.

In the second mode (*m2*), GW adopts parameter values that make the model work as one would expect STD to function (i.e., the model functions with parameters that render GW nonfunctional) (Fig. 8b). Relatively high values of the reciprocal of the e-folding depth of hydraulic conductivity (*fff*) effectively seal the bottom of the soil column, limiting communication between the aquifer and the soil column; high porosity (*maxsmc*) decreases the vertical conductivity, further inhibiting the already poor communication between the soil and aquifer. High porosity favors decreased direct evaporation. Surface runoff is augmented by a relatively high surface runoff scaling factor *fsatmx*; subsurface runoff is lessened by the relatively low subsurface runoff scaling factor (*rsbmx*).

These alternative behaviors are a possible explanation for the issue identified by Rosero et al. (2009), who showed that despite very good performance of calibrated GW, the model suffered from low robustness (high sensitivity to unmeasurable, errant parameters). The bimodal behavior of GW highlights the need to constrain GW with runoff observations, which will help identify a more consistent, better model.

5.4 What changes in DV to make it work better than or as well as STD at site 7?

DV and STD differ functionally in two ways: 1) DV predicts (rather than prescribes) *shdfac* as a function of environmental variation in moisture and radiation availability, and 2) rather than use a temporally constant, prescribed *lai*, DV uses *shdfac* to predict *lai* variation using a functional relationship:

$$lai = \max\left(xlai_{\min}, \frac{-1}{gl} \log^{-1}(1 - shdfac) \right) \tag{14}$$

The vegetated fraction affects all three components of LE: vegetation shades the soil, modulating direct evaporation (E_{dir}); vegetation retains water above the soil, contributing to evaporation from the canopy (E_c); vegetation fuels transpiration (E_{transp}). Because of *shdfac*'s role in scaling all components of evapotranspiration, a high value of conversion parameter *gl* yields a regime in which E_c and E_{transp} are strongly favored over E_{dir}. Low values of *gl* fix *shdfac* near zero and promote a regime in which E_{dir} is the dominant component of LE. When *shdfac* is near zero, both E_c and E_{transp} are minimized. At sites with sufficient vegetation, DV enables the model to correctly give more weight to E_{transp}. When there is little vegetation (e.g., at sites 1-3), the coupling to DV may be failing to consider special water use features associated with the semi-arid vegetation (Unland et al., 1996).

STD keeps *shdfac* fixed at monthly climatological values (~0.7 at site 7) and does not relate *shdfac* to *lai*. STD, unable to change the value of *shdfac* to shift the balance of components of LE, favors higher *lai* (which decreases stomatal resistance and increases E_{transp}) as means for increasing total LE.

When compared to STD, DV can achieve 'good' model performance using a wider range of values for *shdfac* and *lai*. We see this decreased identifiability of DV parameters when comparing the bivariate posterior parameter distributions of STD to those of DV at site 7 (Fig. 9). The identifiability in the response surface of RMSE LE has changed (e.g. *lai* vs. *rcmin*). The decrease in identifiability of parameters that are functionally related to *shdfac* and/or *lai* can be seen across the IHOP sites (results not shown).

The interplay of the parameters of the DV module also leads to changes in parameter densities of STD and DV (Fig. 9). We see additional evidence for increased interaction between parameters in DV when we note that the models' covariance structure has been altered (Table 5). For example, *rcmin* and *maxsmc* are positively correlated in STD, but in DV they have a very slight negative correlation.

Although the increased flexibility of *lai* and *shdfac* values may improve the model's simulation of seasonal and interannual variation in surface fluxes, over time scales examined here, DV does not appear to improve the model. The constraints imposed by the turbulent and near-surface states may be insufficient for the complexity of the model and/or DV may need to be constrained with observations of carbon fluxes and plant growth. The function of the DV module may be hindered by Noah's lack of a separate canopy layer (Rosero et al., 2009) or the absence of a more complex Ball-Berry type of stomatal conductance formulation (Niu et al., 2009).

6. What does sensitivity analysis tell us about transferability?

LSM parameters are frequently assumed to be physical quantities, which can be measured and which have strong relationships with physical properties of the system. These assumptions imply that optimal values should not vary between models and that relationships between model parameters should be constant between models and between sites with similar physical properties. By making sets of vegetation-related parameters functions of vegetation type, LSMs contain the implicit assumption that vegetation type solely determines the ideal values of vegetation parameters. A priori assignment of parameter values based on a site's physical characteristics ('parameter transferability') depends on the above assumption. Our VSA shows that interaction between parameters contributes most to a LSM's total variance causing optimal parameter values to change significantly between models and sites. If parameters are transferable between similar sites, then the relationships between parameters should also be transferable between similar sites. The joint multivariate posterior distribution summarizes much of the information regarding the relationships between model parameters (model structure) at a particular location given observed datasets. We use the stable posterior distributions of the behavioral parameter sets to test the assumption that parameters and parameter relationships relate directly to physical characteristics. We also evaluate the extent to which climate determines the similarity of parameters between locations.

6.1 Testing parameter transferability between sites using soil and vegetation types

If parameters were readily 'transferable' between sites solely based on the vegetation class, we would expect the distributions of the vegetation parameters at two sites with the same vegetation type but different climatic regime (e.g., sites 2 and 8) to be more similar than the distributions of the same parameters at two sites with different vegetation but similar climate (e.g., sites 2 and 1). Using evidence from the marginal posterior parameter distributions of behavioral, sensitive, 'physically meaningful' vegetation parameters (*rcmin*, *lai*, and *sbeta*), Figure 10 shows that this expectation does not hold. Figure 10 contrasts the vegetation parameters' posterior distributions for sites 2 and 8 (grassland) against the posterior distributions for contiguous sites 1 and 2 (dry). The distributions of *rcmin*, *rsmax*, *lai* and *z0* are more similar between sites with similar climate than they are between sites with the same vegetation (Fig. 10a, 10b). *hs* and *cmcmax* show a similar lack of transferability. Only *sbeta* shows 'transferability' (i.e., there are smaller differences between the distributions from sites with the same vegetation cover) for all models (Fig. 10c). Parameter *cfactr* does show transferability, but only for STD. *rgl* could be considered 'transferable,' but only for DV and GW.

Using the IHOP dataset, we cannot test parameter transferability using two sites with the same soil type but different climatology. We instead tested whether the distributions of soil parameters transfer along with soil or vegetation characteristics between these sites. Only *fxexp* appears 'transferable' between dry sites (1 and 2) with the same soil type (sandy clay loam) in STD and GW (Fig. 11b). Some parameters have more similar distributions between sites 2 and 8 than between sites 1 and 2: *psisat* and *satdk* only for GW, Clapp and Hornberger's *b* only for STD, *maxsmc* for STD and GW (Fig. 11a), and *czil* for STD and DV (Fig. 11a). Perhaps this is because, despite sharing the same soil type, site 1 received more than twice the amount of precipitation observed at site 2. We also hypothesize that transferability based on soil or vegetation type is not uniformly viable because of the interactions between soil and vegetation parameters, which condition the shape of the distributions. The interactions between the soil and vegetation parameters at grassland site 2 are significantly different than the interactions at unvegetated site 1.

We recognize that the case studies above are by no means conclusive, but they do not support the hypothesis that parameters are transferable solely based on vegetation type. The results instead suggest that land-surface model parameters are more sensitive to climatic forcing than to a specific soil or land-cover classification. Such results provide support to similar observations made about other hydrologic models (Demaria et al., 2007; van Werkhoven et al., 2008) and made about the Noah LSM and using single optimal parameter sets (Hogue et al., 2005; Rosero and Bastidas, 2007) .

6.2 Synthesizing sensitivity to site, soil and vegetation classes by means of clustering

In order to more quantitatively synthesize knowledge gained through sensitivity analysis for use at ungauged locations, we build upon the aforementioned idea of comparing the similarity of parameter distributions across sites (Rosero and Bastidas, 2007) by complementing the approach with unsupervised, agglomerative hierarchical clustering methods.

For each IHOP site, we have obtained a stable, multivariate probability distribution χ of behavioral parameter sets X={x_1, x_2, …, x_i, …x_k} using multi-objective parameter estimation. The marginal probability distribution for the i^{th} parameter is χ_i. To circumvent comparing between sites against each other (two at a time, as done above), we define a triangular probability distribution D_i as a reference distribution for each parameter. D_i=1 when the value of parameter x_i is the "default" for the site. D_i=0 when x_i is at either edge of the feasible range. This step allows us to introduce the assumption that the parameters relate to soil and vegetation types.

For each parameter, and at each site, we quantify the closeness between the cumulative distribution of the 'optimal' values of x_i (i.e, the marginal χ_i) and the reference D_i. We use the Hausdorff norm to quantify the difference $\chi_i - D_i$. For each model, the matrix of 'signatures' of the marginal distributions of k parameters at all the n evaluation sites is:

$$S = \begin{bmatrix} \chi_{11} - D_{11} & \cdots & \chi_{k1} - D_{k1} \\ \cdots\cdot & \cdots & \cdots \\ \chi_{k1} - D_{k1} & \cdots & \chi_{kn} - D_{kn} \end{bmatrix} \tag{15}$$

S can be used to identify groups of parameters that are similar between locations or to identify locations where groups of parameters behave alike. We use the unsupervised, agglomerative hierarchical clustering algorithm (described in Section 2.8) to find these groups without making any further assumptions about the number of groups.

The Noah LSM works with three classes of parameters: parameters associated with soil type (soil parameters), parameters associated with vegetation cover type (vegetation parameters), and general parameters. If the previously described assumption of parameter transferability based on site characteristics holds (and if IHOP vegetation classifications are correct), then, given the set of signature vectors created using the set of vegetation parameter distributions $S(x_{\mathrm{veg},1..n})$, a clustering procedure should be able to classify similar sites in groups that resemble the IHOP vegetation type groupings (Table 1). Similarly, clustering of $S(x_{\mathrm{soil},1..n})$ would result in sites grouped according to the IHOP soil type classification (Table 1).

Applying a suite of distance metrics (e.g., Manhattan, Euclidean, Cosine, etc), neither soil nor vegetation parameters render groups of sites that partition solely based on the expected soil or vegetation classifications. Figure 12a shows the classification tree (dendrogram) for STD using the Euclidean distance, which maximizes the cophenetic correlation coefficient of the linkage (also shown). None of the distance metrics allowed us to classify $S(x_{\mathrm{veg},1..n})$ by location in a way that matched the IHOP vegetation classifications. Given the subset $\mathrm{S}(x_{\mathrm{soil},1..n})$, composed of the signature vectors of the 10 soil parameters at all sites, classification of the IHOP sites according to soil characteristics was also not feasible (Fig. 12b). Using signature vectors for STD, GW, and DV, some (but not all) of the distances related sites 7, 8, and 9 as having the same soil and same vegetation type (although, because they also share the same climate type, we are unable to definitively attribute such classification to shared vegetation type). The rest of the sites do not strongly coalesce according to physical properties. For example, the pasture sites are not distinctively together; sites 5 and 6 (wheat crops) are never classified together according to vegetation (Fig 12a). Sites 1 and 2 (sandy clay loam) and sites 4 and 5 (loam) do not cluster together using soil parameters (Fig 12b). These results support the earlier findings presented here, which suggest that interaction between soil and vegetation parameters is significant, to the point that it shapes the posterior parameter distributions. These results also suggest that soil and vegetation type are not, by themselves, good physical characteristics by which to transfer parameters.

Next, to account for the interdependence between soil and vegetation parameters, we classified the entire matrix $S(x_{soil},x_{veg})$. If parameters can be transferred based on shared vegetation and soil type, then the clustering of the entire matrix should identify groups of sites with the same vegetation and soil type (e.g, sites 7-9). Figure 12c shows a pattern (found with several distances) that is consistent across models: sites 7-9 cluster together. Sites 7, 8, and 9 have also similar climates, and the classification of the sites shows strong resemblance to the climatic gradient. Given this dataset, we cannot disprove the contention that parameters can be transferred between sites that have both the same vegetation type and the same soil type.

If we instead cluster S looking for groups of parameters, the expectation is that x_{soil} will behave as a whole in a similar way across sites. In other words, one can produce a map of sensitivity to characterize which parameters are most similar to their default (prior distribution) and which are not. Figure 13 shows representative groupings of the behavioral, marginal posterior distributions of STD and GW parameters at all sites. Again, using a suite of distances, we were unable to identify definitive clusters of soil and vegetation parameters within the set of signature vectors *S*, meaning that individual parameters are not sensitive in groups that relate primarily to soil or vegetation, but to a combination of both. The new GW parameters do seem to behave in a way that is similar to other soil parameters (Fig. 13b), which informs the estimation of these parameters for distributed applications.

We conclude that the primary site-to-site control on the parameters identified as 'vegetation' or 'soil' parameters is not a site's type of soil or vegetation used in isolation. This is consistent with the notion that given that parameters used by LSMs must represent physical processes across multiple scales, the parameters become "effective" rather than physically derived quantities (Wagener and Gupta, 2005) and that interaction between classes of parameters are very important. Our clustering analysis suggests that climate is a major control of site-to-site variation in parameter values and supports recommendations that mean climate be considered when transferring parameter values between sites (Liang and Guo, 2003; Demaria et al., 2007; vanWerkhoven et al., 2008).

7. Summary and Conclusions

We combine two powerful sensitivity analysis methods, regionalized sensitivity analysis (RSA) and global variance-based sensitivity analysis (VSA), to inform model identification and development. We draw conclusions regarding LSM development and model assessment practices, the functioning of three versions of the widely used Noah LSM, and the a priori assignment of parameter values. Our work yields several conclusions that can be generalized to all LSM and to other environmental models and several others that are specific to the Noah LSM.

We show that VSA complements RSA for the purposes of model development. We perform VSA and RSA on a single set of Monte Carlo runs. When used together, VSA and RSA help developers understand model behavior (i.e., how and when different modules interact, how a model varies in performance between climate regimes, how a model performs differently between sites, how different models perform at the same site, etc.). SA identifies parameters whose behavior merits further examination: VSA identifies parameters responsible for model uncertainty; RSA identifies modes in parameter distributions that yield distinctive behavior.

We show that the clear patterns of parameter importance identified by VSA are consistent with site-to-site variation in climate and with model-to-model changes in physical parameterization. VSA shows that parameter interactions within models exert significant control on model variance, and we show that the interactions can be traced using RSA. Shifts in parametric control on variance and covariance hint at whether a model represents the water and energy cycles in a way that is consistent with expectations. Although the optimal value of a parameter is useful information, the change in the functional relationship between parameters is more relevant for model development and hypothesis testing. We assert that to advance model development, VSA should be used in conjunction with RSA.

Transfer of parameters based solely on shared vegetation type or on shared soil type is not a viable method for a priori parameter assignment. The work presented here shows that vegetation type and soil type are not the most significant contributors to site-to-site variance in optimal parameter values. Interaction between soil and vegetation parameters is significant and varies between sites; parameter interaction at least partially explains why transfer of parameters based solely on shared vegetation or soil type does not work. The primary factor controlling site-to-site variation in parameters is likely climate, although, given the dataset used here, the combination of a site's vegetation and soil type or some unidentified factor cannot be ruled out as the dominant controlling factor. The lack of viability of parameter transfer based solely on soil and vegetation type is a conclusion that has significant implications for the field of regional and global land surface modeling, which depends on parameter transfer based on stand-alone vegetation type and soil type as a means for a priori parameter assignment.

Looking specifically at the performance of the three versions of the Noah LSM used here (STD, GW, and DV), we make several non-site-specific conclusions regarding model behavior. All three models exhibit significant parameter interaction, indicating that the models are overparameterized and/or underconstrained. All three show the least parameter interaction at the middling-moisture and wet sites and the most parameter interaction at the three driest sites. This difference suggests a need for reformulation of Noah LSM such that semi-arid regions are more realistically represented. On the whole, GW has less parameter interaction than STD (except at dry sites), indicating that it represents land-surface system with the most realism of any of the three models. GW is also least sensitive to errant parameters at the wettest sites (where groundwater is likely the most influential). DV has much more parameter interaction than STD, which provides evidence that the model is not performing as its developers intended, does not add value to STD, and/or requires additional constraint. Specific to site 7, we make the following observations: STD and DV tend to underestimate direct evaporation from the soil; GW does not (maybe because of wet soil). The assumption that vegetation decreases the thermal conductivity of the top layer of the soil is not well supported by data (this conclusion can be roughly generalized to other sites, especially the wet sites). At site 7, GW functions in one of two modes – the slightly preferred mode works in a way that mirrors what the developers likely intended; the second mode makes GW function as one might expect STD to work. Constraining runoff may isolate the more realistic mode. GW has less spurious parameter interaction in part because it decouples direct evaporation and subsurface runoff (which are coupled via porosity in STD and DV). This decoupling appears to make the model function more realistically, with less tradeoff between the simulation of soil moisture and LE. Adding modules (DV, GW) decreases the identifiability of minimum stomatal resistance, although all three models prefer low minimum stomatal resistance (thus increasing LE for a given set of conditions). Across several sites, DV functions in one of two modes: the first emphasizes direct soil and canopy evaporation over transpiration; the second emphasizes transpiration over direct evaporation from the soil and canopy.

Our approach to sensitivity analysis complements new methods for characterizing typical modes of LSM behavior (Gulden et al., 2008b; Rosero et al., 2009) within a model diagnostic framework (Gupta et al., 2008) that helps bridge the gap between model identification and development. We encourage other modeling groups to perform similar analyses with their models as a way to ensure rapid, continued improvement of our understanding and modeling of environmental processes.

Acknowledgements We thank Pedro Restrepo at OHD/NWS, Dave Gochis at NCAR and Ken Mitchell at NCEP for their insight. We appreciated suggestions by M. Bayani Cardenas, Charles S. Jackson and Yasir H. Kaheil. We acknowledge the International H_2O Project for the datasets. We benefited from the computational resources at the Texas Advanced Computing Center (TACC). This project was funded by the Graduate Fellowship of the Hydrology Training Program of the OHD/NWS, the NOAA grant no. NA07OAR4310216, NSF, and the Jackson School of Geosciences.

REFERENCES

Abramowitz, G., Pitman, A. J., Gupta, H., Kowalczyk, E. and Wang, Y., (2009). On the need for a biophysically based benchmark for land surface models, *J. Hydrometeor*., accepted.

Asefa, T., M. W. Kemblowski, G. Urroz, M. McKee, and A. Khalil (2004), Support vectors–based groundwater head observation networks design, *Water Resour. Res.*, *40*(11), W11509, doi:10.1029/2004WR003304

Asefa, T., M. Kemblowski, U. Lall, and G. Urroz (2005), Support vector machines for nonlinear state space reconstruction: Application to the Great Salt Lake time series, *Water Resour. Res.*, 41, W12422, doi:10.1029/2004WR003785.

Asefa, T., Kemblowski, M. W., McKee, M., & Khalil, A. (2006). Multi-time scale stream flow prediction: The support vector machines approach. *J. Hydrol.*, 318, 7–16.

Bastidas, L.A., H.V. Gupta, S. Sorooshian., W. J. Shuttleworth, and Z. L. Yang, 1999: Sensitivity analysis of a land surface scheme using multicriteria methods, *J. Geophys. Res.*, ***104***(D16), 19,481–19,490

Bastidas, L.A., H.V. Gupta, and S. Sorooshian., 2001: Bounding the parameters of land-surface schemes using observational data. *Land surface hydrology, meteorology, and climate: Observations and Modeling*. V. Lakshmi et al. (ed.), Water Science and Application, Vol.3, AGU, 65–76.

Bastidas, L.A., T. S. Hogue, S. Sorooshian, H. V. Gupta, and W. J. Shuttleworth, 2006: Parameter sensitivity analysis for different complexity land surface models using multicriteria methods, *J. Geophys. Res.*, **111**, D20101, doi:10.1029/2005JD006377.

Beven, K. J., and Freer, J., 2001: Equifinality, data assimilation, and uncertainty estimation in mechanistic modelling of complex environmental systems, *J. Hydrol.*, 249, 11–29

Beven, K. J. and Freer, J., 2001: Equifinality, data assimilation, and uncertainty estimation in mechanistic modelling of complex environmental systems, *J. Hydrol.*, 249, 11-29.

Chen, F., and J. Dudhia, 2001: Coupling an Advanced Land Surface–Hydrology Model with the Penn State–NCAR MM5 Modeling System. Part I: Model Implementation and Sensitivity. *Mon. Wea. Rev.*, **129**, 569–585.

Cosgrove, B. A., et al. (2003), Real-time and retrospective forcing in the North American Land Data Assimilation System (NLDAS) project, *J. Geophys. Res.*, **108**(D22), 8842, doi:10.1029/2002JD003118.

Demaria, E. M., B. Nijssen, and T. Wagener, 2007: Monte Carlo sensitivity analysis of land surface parameters using the Variable Infiltration Capacity model, *J. Geophys. Res.*, **112**, D11113, doi:10.1029/2006JD00

Demarty, J., C. Ottlé, I. Braud, A. Olioso, J. P. Frangi, L. Bastidas, and H. V. Gupta, 2004: Using a multiobjective approach to retrieve information on surface properties used in a SVAT model, *J. Hydrol.*, *287*, 214–236

Dickinson, R.E., M. Shaikh, R. Bryant, and L. Graumlich, 1998: Interactive Canopies for a Climate Model. *J. Climate*, **11**, 2823–2836.

Dibike, B. Y., S. Velickov, D. Solomatine, and B. M. Abbot (2001), Model induction with support vector machines: Introduction and applications, *J. Comput. Civ. Eng.*, *15*, 208–216

Duan, Q., V. K. Gupta, and S. Sorooshian (1992), Effective and efficient global optimization for conceptual rainfall-runoff models, *Water Resour. Res.*, *28*(4), 1015–1031

Ek, M.B., et al., 2003: Implementation of Noah land surface model advances in the National Centers for Environmental Prediction operational mesoscale Eta model. *J. Geophys. Res.*, **108**(D22), 8851, doi:10.1029/2002JD003296.

Gill, M. K., T. Asefa, Y. Kaheil, and M. McKee (2007), Effect of missing data on performance of learning algorithms for hydrologic predictions: Implications to an imputation technique, *Water Resour. Res.*, 43, W07416, doi:10.1029/2006WR005298

Gulden, L.E., E. Rosero, Z.-L. Yang, M. Rodell, C.S. Jackson, G.-Y. Niu, P. J.-F. Yeh, and J. Famiglietti, 2007: Improving land-surface model hydrology: Is an explicit aquifer model better than a deeper soil profile? *Geophys. Res. Lett.*, **34**, L09402, doi:10.1029/2007GL029804

Gulden, L. E., Z.-L., Yang, and G.-Y. Niu, (2008a), Sensitivity of biogenic emissions simulated by a land-surface model to land-cover representations, *Atmos. Env.*, doi:10.1016/j.atmosenv.2008.01.045

Gulden, L. E., E. Rosero, Z.-L. Yang, T. Wagener, and G. Niu (2008b), Model performance, model robustness, and model fitness scores: A new method for identifying good land-surface models, *Geophys. Res. Lett.,* 35, L11404, doi:10.1029/2008GL033721

Gupta, H.V., S. Sorooshian, and P.O. Yapo, Toward improved calibration of hydrologic models: Multiple and non-commensurable measures of information, *Water Resour. Res.,* **34**(4), 751-763, 1998

Gupta, H.V., L.A. Bastidas, S. Sorooshian, W.J. Shuttleworth and Z.L. Yang, 1999: Parameter estimation of a land surface scheme using multicriteria methods. *J. Geophys. Res.*, **104**(D16), 19491-19504.

Gupta, H.V., T. Wagener, Y. Liu (2008), Reconciling theory with observations: Elements of a diagnostic approach to model evaluation, *Hydrological Processes*, 22, doi:10.1002/hyp.6989.

Gao, X., S. Sorooshian, and H. V. Gupta (1996), Sensitivity analysis of the biosphere-atmosphere transfer scheme, *J. Geophys. Res.*, 101(D3), 7279–7289.

Helton, J., and F. Davis, 2003, Latin hypercube sampling and the propagation of uncertainty in analyses of complex systems, *Reliab. Eng. Syst. Safety*, **81**(1), 23– 69.

Hair, J. F., Anderson, R. E., Tatham, R. L., Tatham, R. L. & Black, W. C. (1995). Multivariate Data Analysis with Readings. Prentice-Hall: Upper Saddle River, NJ.

Hornberger, G. M., and R. C. Spear (1981), An approach to the preliminary analysis of environmental systems, *J. Environ. Manage.*, *12*, 7–18.

Hogue T.S., L. A. Bastidas, H.V. Gupta, S. Sorooshian, K. Mitchell and W. Emmerich, 2005: Evaluation and Transferability of the Noah Land-surface Model in Semi-arid Environments, *J. Hydrometeor.,* **6**(1), 68–84.

Hogue T.S., L. A. Bastidas, H. V. Gupta, and S. Sorooshian, 2006: Evaluating model performance and parameter behavior for varying levels of land surface model complexity, *Water Resour. Res.*, **42**, W08430, doi:10.1029/2005WR004440

Jakeman, A.J., R.A. Lecter and J. P. Norton, 2006: Ten iterative steps in development and evaluation of environmental models. *Env. Modelling & Software*, 21. 602-614 ,doi:10.1016/j.envsoft.2006.01.004

Joachims T. (1999), Making large-Scale SVM Learning Practical. In *Advances in Kernel Methods - Support Vector Learning,* B. Schölkopf and C. Burges and A. Smola (ed.), MIT-Press.

Kato, H., M. Rodell, F. Beyrich, H. Cleugh, E. van Gorsel, H. Liu, and T.P. Meyers, (2007): Sensitivity of Land Surface Simulations to Model Physics, Land Characteristics, and Forcings, at Four CEOP Sites, *J. Meteor. Soc. Japan*, 85A, 187-204.

Khalil, A., M. N. Almasri, M. McKee, and J. J. Kaluarachchi (2005), Applicability of statistical learning algorithms in groundwater quality modeling, *Water Resour. Res.*, 41, W05010, doi:10.1029/2004WR003608.

Khalil, A., McKee, M., Kemblowski, M. W., Asefa, T., and Bastidas, L.A. (2006). Multiobjective analysis of chaotic dynamics systems with sparse learning machines. *Advances in Water Resources*, 29, 72–88. doi:10.1016/j.advwatres.2005.05.011.

Kaheil, Y. H., M. K. Gill, M. McKee, L. A. Bastidas, and E. Rosero (2008a),"Downscaling and assimilation of surface soil moisture using ground truth measurements," *IEEE Trans. Geosci. Remote Sens.*, vol. 46, no. 5, pp. 1375–1384, May 2008. DOI: 10.1109/TGRS.2008.916086

Kaheil, Y. H., Rosero, E., Gill, M. McKee, and L. A. Bastidas (2008b), Downscaling and Forecasting of Evapotranspiration Using a Synthetic Model of Wavelets and Support Vector Machines. *IEEE Trans. Geosci. Remote Sens*, vol.46, no.9, pp. 2692-2707, Sep. 2008. DOI: 10.1109/TGRS.2008.919819

Koster et al., 2004: Regions of Strong Coupling Between Soil Moisture and Precipitation, *Science,* 305 (5687), 1138.

LeMone, M. A., et al. (2007), NCAR/CU surface, soil, and vegetation observations during the International H2O Project 2002 field campaign, *Bull. Amer. Meteor. Soc.,* **88**, 65-81.

Leplastrier, M., A. J. Pitman, H. Gupta, and Y. Xia, 2002: Exploring the relationship between complexity and performance in a land surface model using the multicriteria method, *J. Geophys. Res.*, ***107***(D20), 4443, doi:10.1029/2001JD000931.

Liang, X., and J. Guo, 2003: Intercomparison of land surface parameterization schemes: Sensitivity of surface energy and water fluxes to model parameters, *J. Hydrol.*, 279, 182-209

Martinez, W and Martinez A. (2002), Computational Statistics Handbook with MATLAB.Chapman and Hall/CRD. ISBN:1584885661 2nd ed. - Boca Raton, Fla. : Chapman & Hall/CRC, 767 p

McKay, M., R. Beckman, and W. Conover (1979), A comparison of three methods for selecting values of input variables in the analysis of output from a computer code, *Technometrics*, *21*(2), 239–245 doi:10.2307/1268522

Mitchell, K. E., et al. (2004), The multi-institution North American Land Data Assimilation System (NLDAS): Utilizing multiple GCIP products and partners in a continental distributed hydrological modeling system, *J. Geophys. Res.,* **109,** D07S90, doi:10.1029/2003JD003823.

Niu, G.-Y., Z.-L. Yang, R.E. Dickinson, and L.E. Gulden, 2005: A simple TOPMODEL-based runoff parameterization (SIMTOP) for use in GCMs, *J. Geophys. Res*, **110**, D21106, doi:10.1029/2005JD006111.

Niu, G.-Y., Z.-L. Yang, R.E. Dickinson, L.E. Gulden, and H. Su, 2007: Development of a simple groundwater model for use in climate models and evaluation with GRACE data, *J. Geophys. Res*., **112,** D07103, doi:10.1029/2006JD007522

Niu, G.-Y., Yang, Z.-L., et al. (2009) The Community Noah Land-Surface Model with Multi-Physics Options, *J. Geophys. Res.,* (submitted)

Oleson, K. W., G. B. Bonan, J. Feddema, M. Vertenstein, (2008) An urban parameterization for a global climate model. Part II: Sensitivity to input parameters and the simulated urban heat island in offline simulations. *J. Appl. Meteor. Climat.*, 47, 1061-1076, doi: 10.1175/2007JAMC1598.1.2

Pitman, A., 1994: Assessing the Sensitivity of a Land-Surface Scheme to the Parameter Values Using a Single Column Model. *J. Climate*, **7**, 1856–1869.

Pitman, A. J., (2003) Review: the evolution of, and revolution in, land surface schemes designed for climate models, *Int. J. Climatol.* **23**, 479–510, doi:10.1002/joc.893.

Prihodko L., A.S. Denning, N.P. Hanan, I. Baker, K. Davis, 2008: Sensitivity, uncertainty and time dependence of parameters in a complex land surface model, *Agric. Forest Meteorol.*, **148**(2), 268-287, doi: 10.1016/j.agrformet.2007.08.006.

Randall, D.A., R.A. Wood, S. Bony, R. Colman, T. Fichefet, J. Fyfe, V. Kattsov, A. Pitman, J. Shukla, J. Srinivasan, R.J. Stouffer, A. Sumi and K.E. Taylor, 2007: Climate Models and Their Evaluation. In: *Climate Change 2007: The Physical Science Basis*. Contribution of Working Group I to the Fourth Assessment Report of the Intergovernmental Panel on Climate Change [Solomon, S., D. Qin, M. Manning, Z. Chen, M. Marquis, K.B. Averyt, M.Tignor and H.L. Miller (eds.)]. Cambridge University Press, Cambridge, United Kingdom and New York, NY, USA.

Ratto, M., P. C. Young, R. Romanowicz, F. Pappenberger, A. Saltelli, and A. Pagano, 2007: Uncertainty, sensitivity analysis and the role of data based mechanistic modeling in hydrology. *Hydrol. Earth Syst. Sci.*, **11**, 1249–1266.

Rodell, M., P. R. Houser, A. A. Berg, and J. S. Famiglietti, 2005: Evaluation of 10 methods for initializing a land surface model, *J. Hydrometeorol.*, ***6***, 146–155.

Rosero, E., and L. A. Bastidas (2007). Evaluation of LSM Parameter Transferability Across Semi-Arid Environments, in Proceedings of the 21st Conference on Hydrology, AMS Meeting, San Antonio, Texas, January 14-18. http://ams.confex.com/ams/pdfpapers/117116.pdf

Rosero E, Yang Z.-L., Gulden L.E., Niu G.-Y., Gochis D.J. (2009) Evaluating Enhanced Hydrological Representations in Noah-LSM over Transition Zones: Implications for Model Development, *J. Hydromet.*, doi: 10.1175/2009JHM1029.1. In Press

Spear R.C. and G.M. Hornberger, (1980). Eutrophication in Peel Inlet-II: Identification of critical uncertainties via generalized sensitivity analysis, *Water Resour. Res.*, 14, pp. 43–99.

Spear, R. C., T. M. Grieb, and N. Shang, 1994. Parameter uncertainty and interaction in complex environmental models, *Water Resour. Res.*, 30(11), 3159-3169.

Smola, A. J., and Schölkopf, B. (2004). A tutorial on support vector regression, Statistics and Computing, 14, 199–222.

Stöckli, R., D. M. Lawrence, G.-Y. Niu, K. W. Oleson, P. E. Thornton, Z.-L. Yang, G. B. Bonan, A. S. Denning, and S. W. Running (2008), Use of FLUXNET in the Community Land Model development, *J. Geophys. Res.*, **113**, G01025, doi:10.1029/2007JG000562.
Sobol', I. M. (1993), Sensitivity analysis for non-linear mathematical models, *Math. Modelling Comput. Exp.*, **1**, 407–414.
Sobol', I. M. (2001), Global sensitivity indices for nonlinear mathematical models and their Monte Carlo estimates, *Math. Comput. Simul.*, **55**, 271–280, doi:10.1016/S0378-4754(00)00270-6
Saltelli, A. (1999), Sensitivity analysis: Could better methods be used?, *J. Geophys. Res.*, *104*(D3), 3789–3793
Saltelli, A., 2002, Making best use of model evaluations to compute sensitivity indices. *Computer Physics Communication*, **145**, 580–297
Saltelli, A., M. Ratto, S. Tarantola, F. Campolongo, 2006, Sensitivity analysis practices: Strategies for model-based inference, *Reliability Engineering & System Safety*, **91**(10-11), 1109-1125
Saltelli, A., M. Ratto, T. Andres, F. Campolongo, J. Cariboni, D. Gatelli, M. Saisana, S. Tarantola, (2008) Global sensitivity analysis: The primer. Wiley-Interscience. ISBN-13: 978-0470059975
Tang, Y., P. Reed, T. Wagener, and K. van Werkhoven (2006), Comparing sensitivity analysis methods to advance lumped watershed model identification and evaluation, *Hydrol. Earth Syst. Sci. Discuss.*, *3*, 3333–3395.
Tang, Y., P. Reed, K. van Werkhoven, and T. Wagener (2007), Advancing the identification and evaluation of distributed rainfall-runoff models using global sensitivity analysis, *Water Resour. Res.*, 43, W06415, doi:10.1029/2006WR005813
Trier, S.B., F. Chen, K.W. Manning, M.A. LeMone, and C.A. Davis, 2008: Sensitivity of the PBL and Precipitation in 12-Day Simulations of Warm-Season Convection Using Different Land Surface Models and Soil Wetness Conditions. *Mon. Wea. Rev.*, **136**, 2321–2343.
Unland, H., P. Houser, W. J. Shuttleworth, and Z.-L. Yang, 1996, Surface flux measurement and modeling at a semi-arid Sonoran Desert site, *Agric. For. Meteorol.*, *82*, 119–153.
van Werkhoven, K., T. Wagener, P. Reed, and Y. Tang (2008), Characterization of watershed model behavior across a hydroclimatic gradient, *Water Resour. Res.*, 44, W01429, doi:10.1029/2007WR006271
van Werkhoven, K., T. Wagener, P. Reed, and Y. Tang (2009), Sensitivity-guided reduction of parametric dimensionality for multiobjective calibration of watershed models, *Adv. Water Resour.*, in press
Vapnik, V. N. (1998), *Statistical Learning Theory*, John Wiley, Hoboken, N. J.
Vrugt, J. A., H. V. Gupta, L. A. Bastidas, W. Bouten, and S. Sorooshian, 2003: Effective and efficient algorithm for multiobjective optimization of hydrologic models, *Water Resour. Res.*, *39*(8), 1214, doi:10.1029/2002WR001746.
Wagener, T., Boyle, D. P., Lees, M. J., Wheater, H. S., Gupta, H. V. and Sorooshian, S. 2001. A framework for development and application of hydrological models, *Hydrol. Earth Syst. Sci.*, **5**, 13-26.
Wagener, T., and H. V. Gupta, 2005: Model identification for hydrological forecasting under uncertainty, *Stoch. Environ. Res. Risk Assess.*, **19**(6), 378– 387, doi:10.1007/s00477-005-0006-5.
Wagener, T., and J. Kollat, 2007: Numerical and visual evaluation of hydrological and environmental models using the Monte Carlo Analysis Toolbox, *Environ. Modell. Softw.*, **2**, 1021–1033
Weckwerth, et al., 2004: An overview of the International H2O Project (IHOP_2002) and some preliminary highlights. *Bull. Amer. Meteor. Soc.*, **85,** 253–277.
Yatheendradas, S., T. Wagener, H. Gupta, C. Unkrich, D. Goodrich, M. Schaffner, and A. Stewart (2008), Understanding uncertainty in distributed flash flood forecasting for semiarid regions, *Water Resour. Res.*, *44*, W05S19, doi:10.1029/2007WR005940
Yang, Z.-L., and G.-Y. Niu, 2003: Versatile integrator of surface and atmosphere processes (VISA) Part 1: Model description. *Glob. Planet. Change* **38**, 175–189

FIGURES

Figure 1. IHOP_2002 near-surface state and flux stations. The contours show the strong east - west mean annual precipitation (MAP) gradient. The nine sites were located in representative land covers (see Table 1): six on grassland of varying thickness, two on winter wheat, one on bare ground, and one on shrubland. The surface temperature of the dry (MAP=550 mm), sparsely vegetated sites (1-3) is mainly linked to the soil moisture. In contrast, the green, lush vegetation of the wet sites (7-9) (MAP=900 mm) controls the surface temperature. In sites 4-6 (MAP=750 mm), a mix of winter wheat and grassland, the surface temperature is influenced by both soil moisture and vegetation.

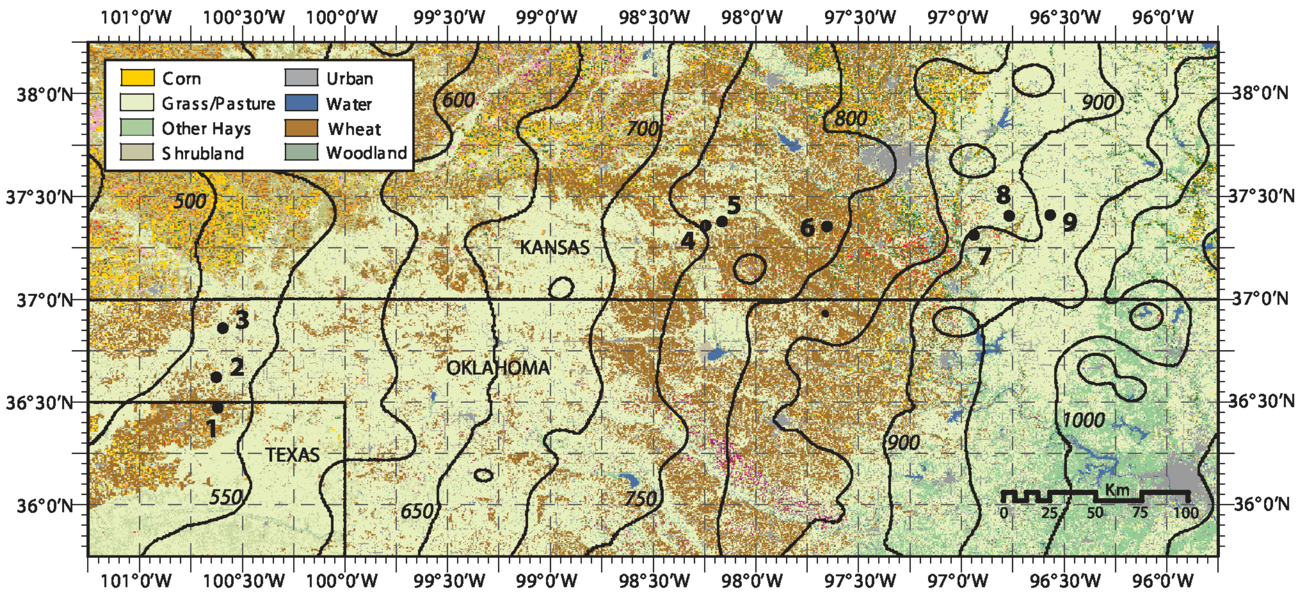

Figure 2. (a) First-order Sobol' sensitivity indices for the parameters of STD, GW and DV at all sites. S_i stands for the individual contribution of a parameter to the variance of the RMSE of H. (b) Difference between Sobol''s total sensitivity index and S_i. S_{Ti} -S_i is the contribution to the variance through interactions with other parameters. Parameters grouped by soil and vegetation. See Table 2 for abbreviations of parameter names. Regional sensitivity patterns from semi-arid (MAP=550 mm), sparsely vegetated sites (1-3) to semi-humid (MAP=900 mm) sites (7-9) with green, lush vegetation, are easily distinguishable.

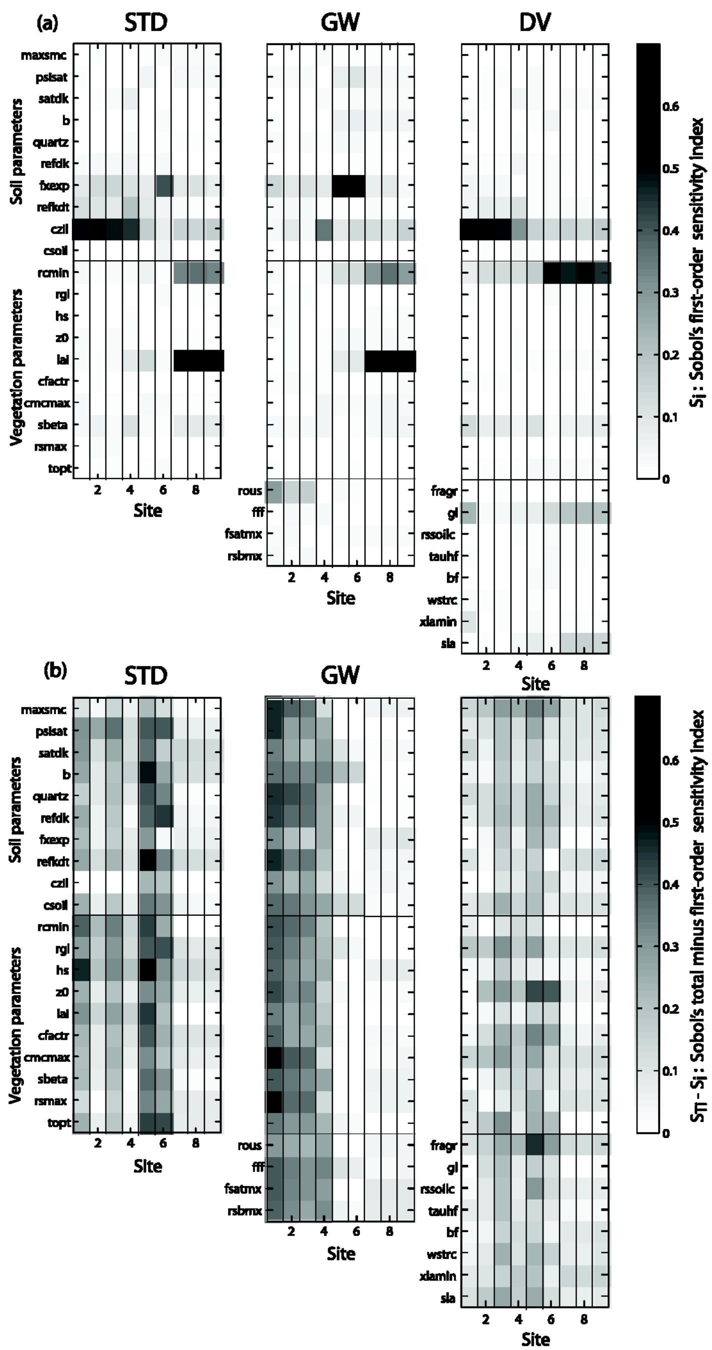

Figure 3. Same as Figure 2 but for LE.

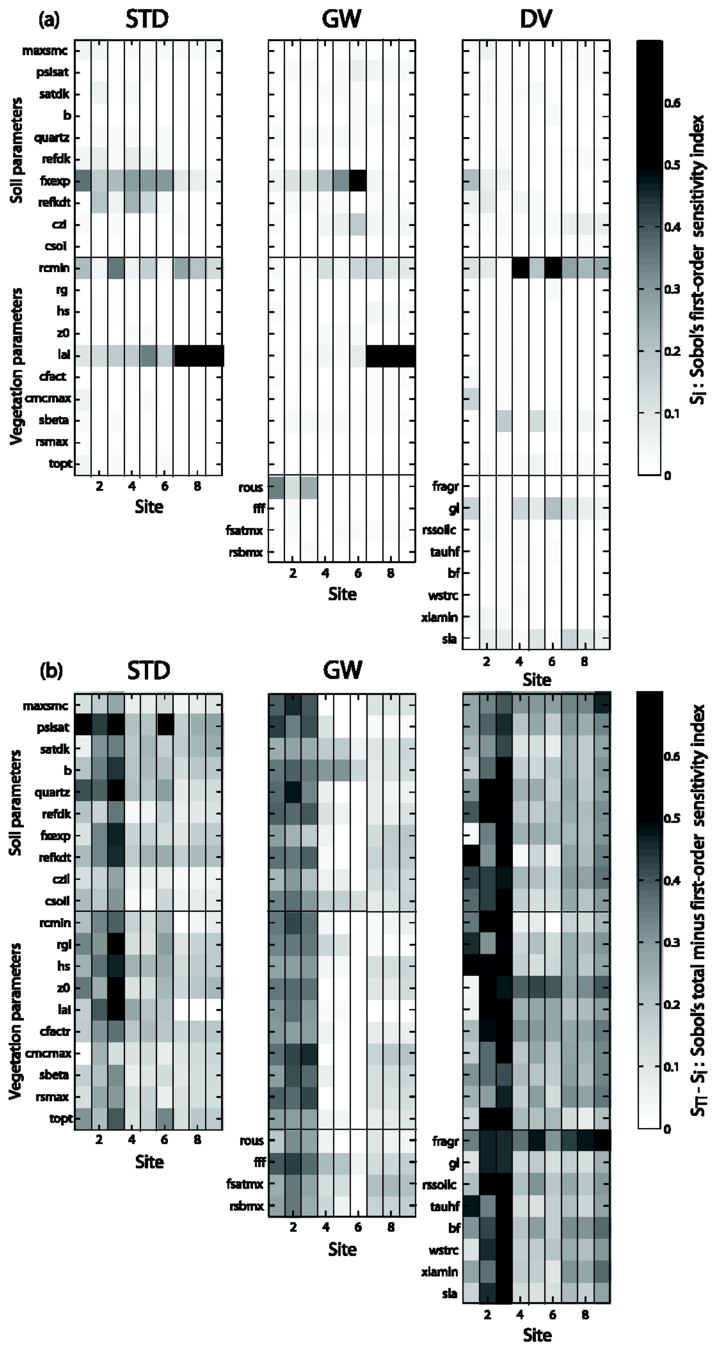

1 **Figure 4.** Same as Figure 2 but for SMC_{5cm}.

2

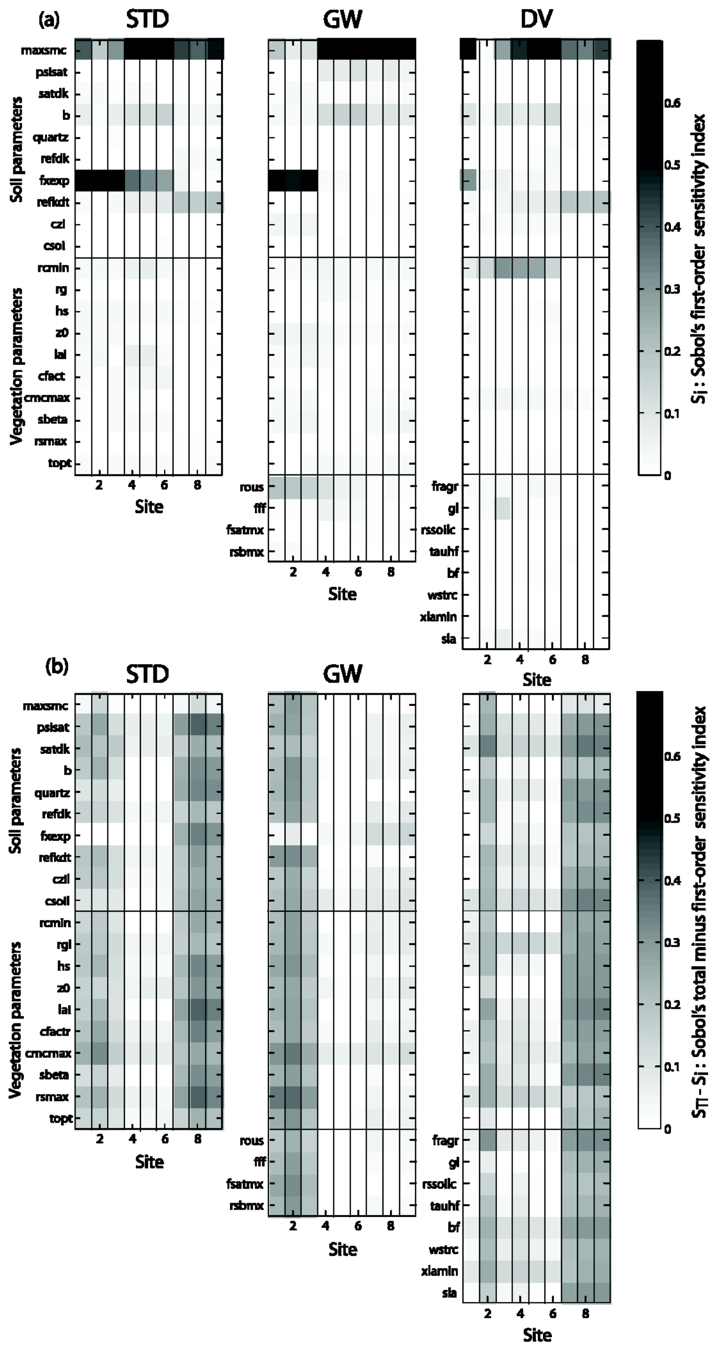

3

Figure 5. Tradeoff LE-SMC_{5cm} and cumulative distribution functions (CDF) of scores of behavioral STD, GW and DV at Site 7. (a) Scatterplot in objective function space of parameter sets that maximize the likelihood function after multi-objective calibration against {H, LE, G, Tg, SMC_{5cm}}. CDF of root mean squared errors (RMSE) of behavioral runs evaluated against observed (b) LE, and (c) SMC_{5cm}. GW (dark grey), DV (light gray) perform as good as or better than STD (black).

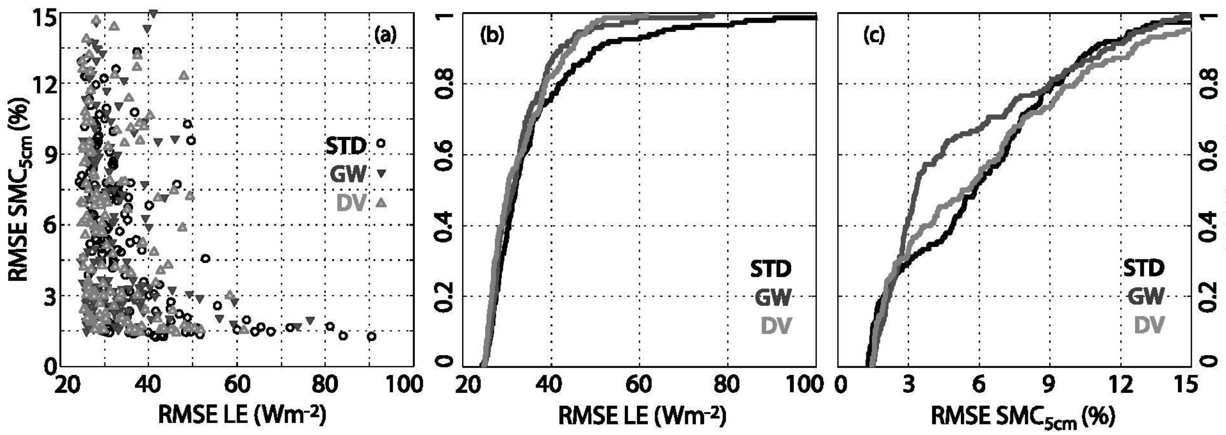

Figure 6. Uncertainty ranges of the 150 ensemble members of behavioral runs of STD (black), GW (dark gray) and DV (light gray) at Site 7. (a) Average diurnal LE. (b) Hourly SMC_{5cm}. Plots show the interquartile range IQR (50% of the runs) in continuous lines and the 90% confidence bounds (5% to 95% quantile) in dashed lines. Observations are shown with symbols. The spread of LE by STD is larger than that of DV, GW. However, IQR shows a very similar LE envelope. The ensemble of GW shows wetter SMC_{5cm} than the rest. The IQR of STD and DV are very similar, but the 90% confidence of STD has lower spread than DV.

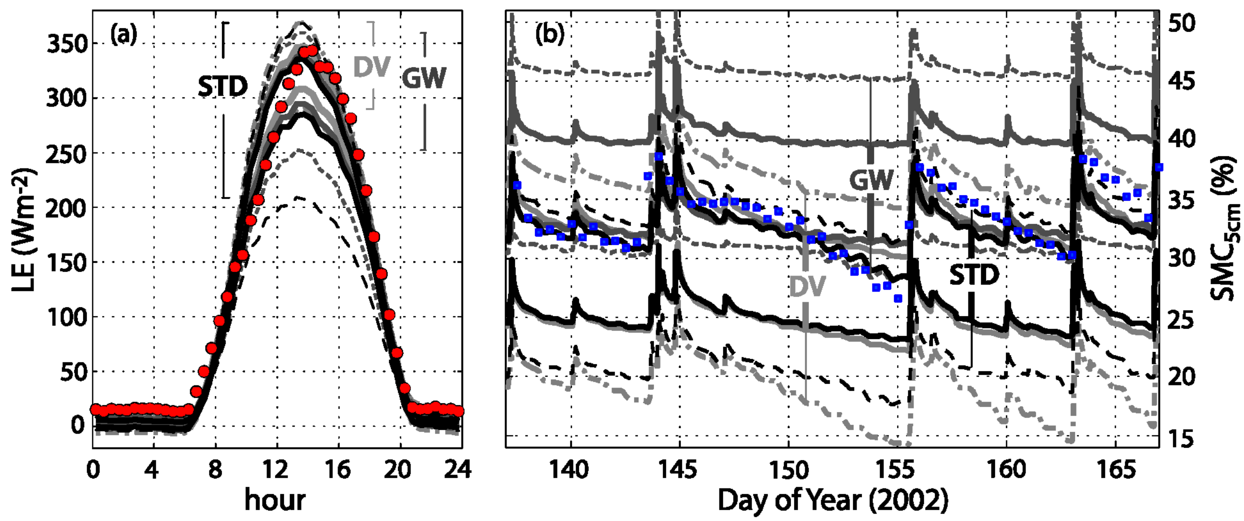

Figure 7. Marginal cumulative distribution functions (CDF) of the posterior distribution of selected behavioral parameter sets at Site 7. (a) Porosity [maxsmc], (b) minimum stomatal resistance [rcmin], (c) maximum water holding capacity of the canopy [cmcmax], and (d) effect of the vegetation on ground heat flux [sbeta]. Along with the CDFS, the histograms and interquartile ranges are also shown. The trend in the scatterplots of RMSE of LE and SMC_{5cm} is shown by fitting a minimum complexity polynomial. Note that in all subpanels GW (dark grey), DV (light gray) and STD (black) are shown.

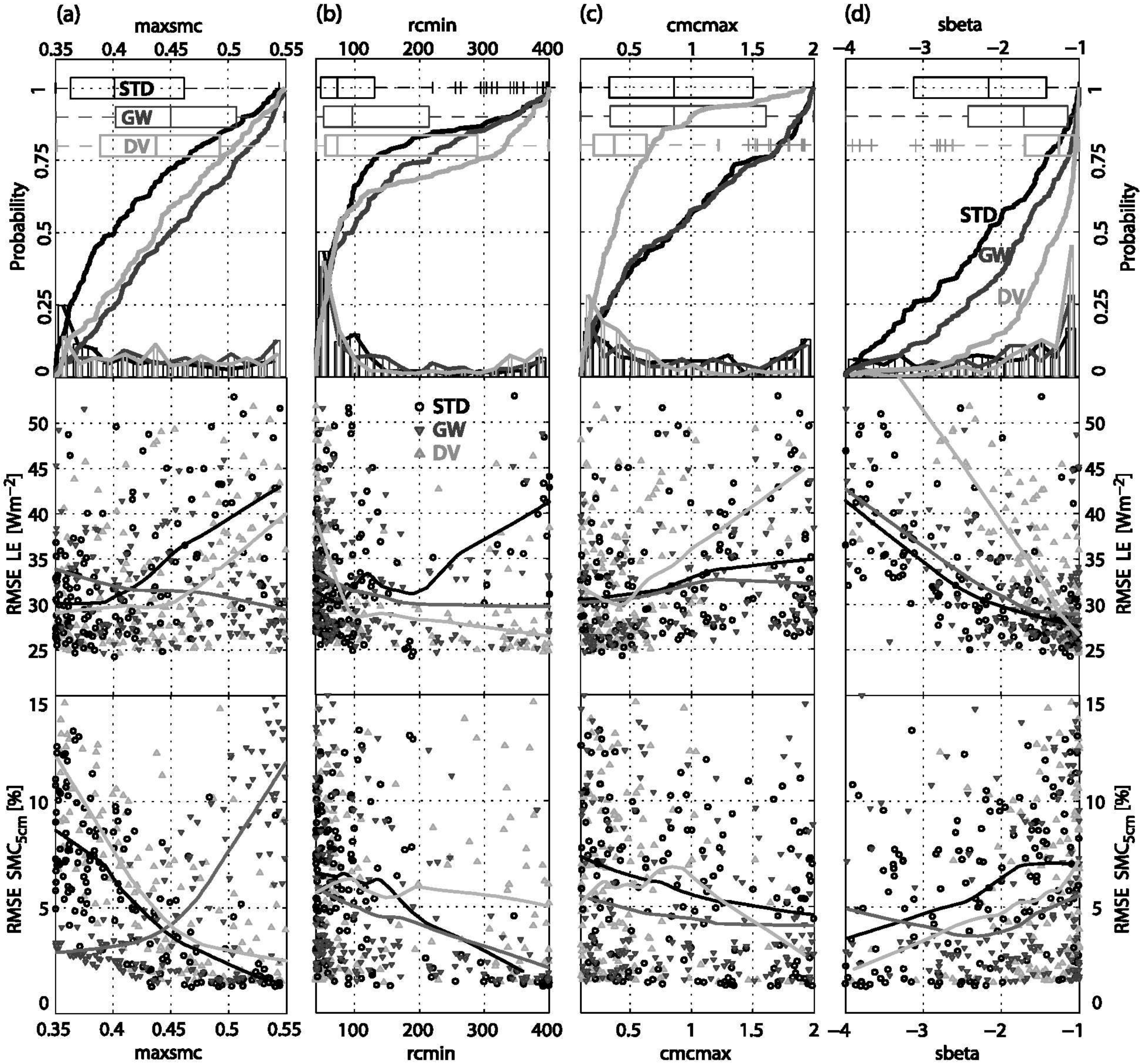

Figure 8. Multivariate posterior distribution of the behavioral parameters of STD and GW at site 7 shown for selected parameter combinations in bivariate plots. Higher density of parameter values are indicated with increasingly redder contours. The response surface of SMC_{5cm} is shown in the back; darker regions have higher errors. The bi-modal behavior of GW is signaled by *m1* and *m2*. See text for explanation.

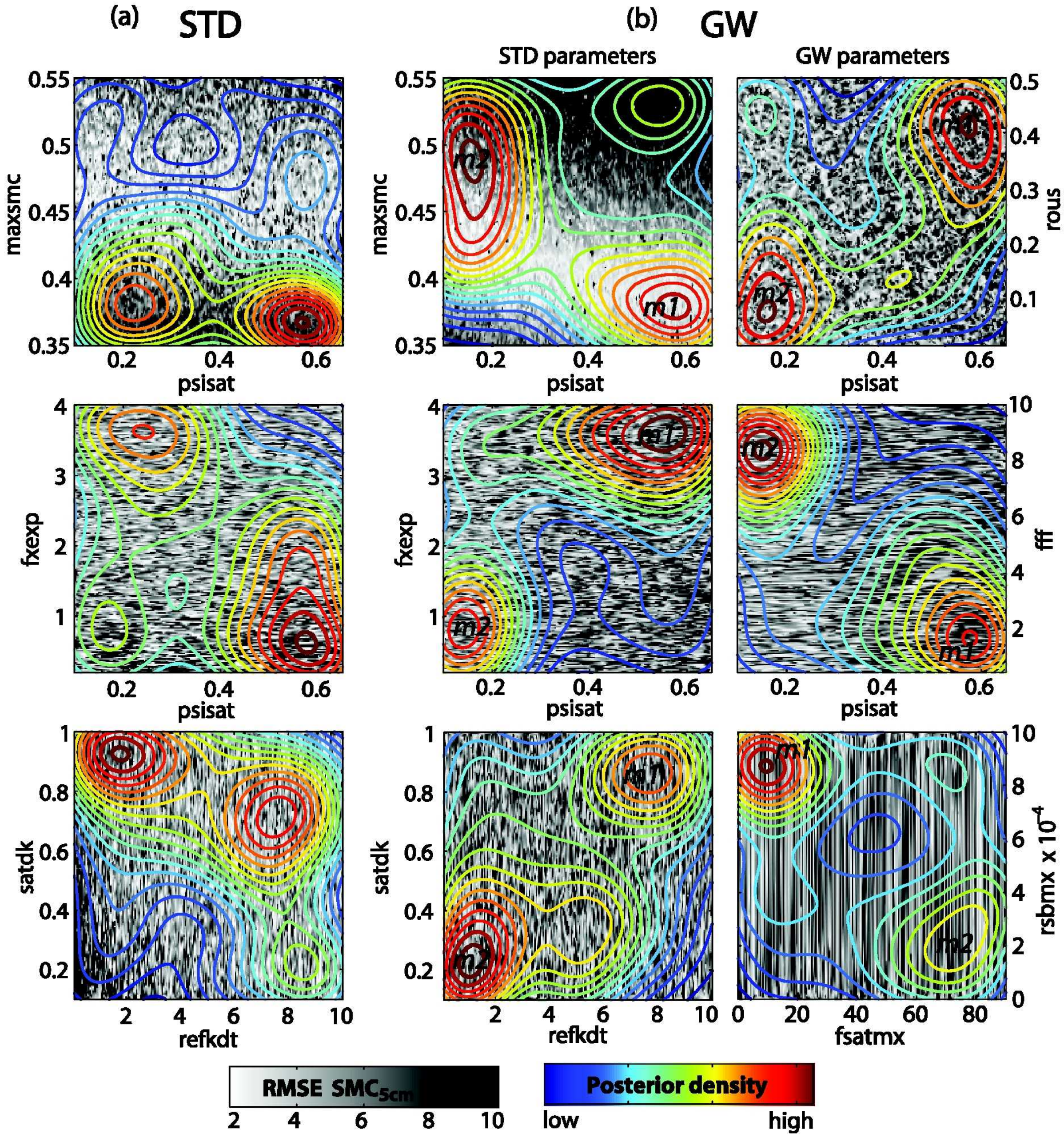

Figure 9. Bivariate depiction of the posterior distribution of behavioral parameters of STD and DV at Site 7. Higher density of parameter values are indicated with red contours. The response surface of LE is shown in the back; darker regions have higher errors. Note the significant change in the identifiability of hs and maxsmc.

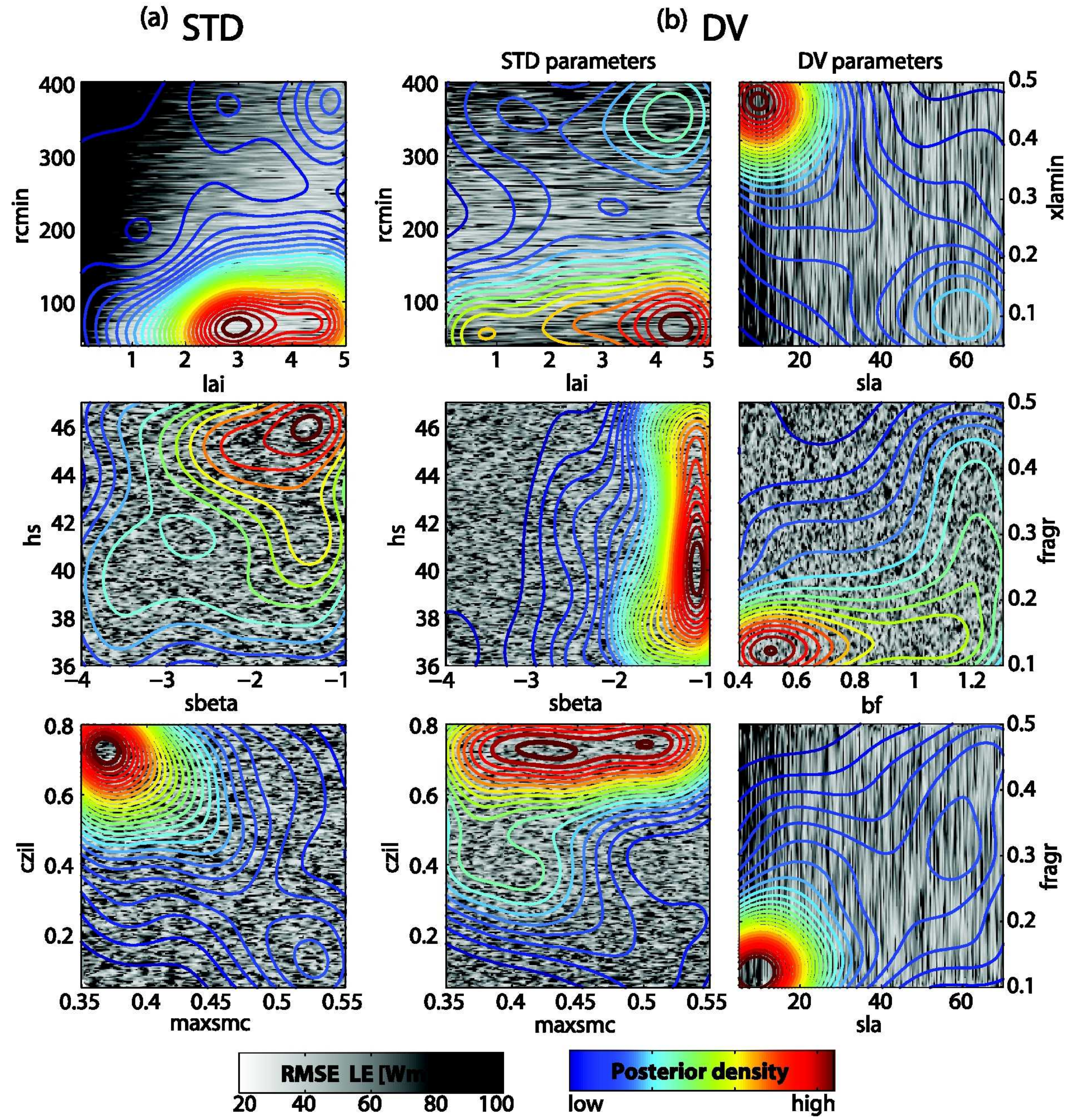

Figure 10. Comparison of the marginal posterior parameter distributions of selected, sensitive vegetation parameters: (a) rcmin, (b) lai, and (c) sbeta. The total difference between parameter distributions at sites with the same vegetation cover type (Site 2 and 8) –grassland– (continuous, bright lines) is not smaller than the difference of distributions of the same parameters between contiguous sites (Site 2 and 1) (dashed, dark lines), which share the same soil type (sandy clay loam).

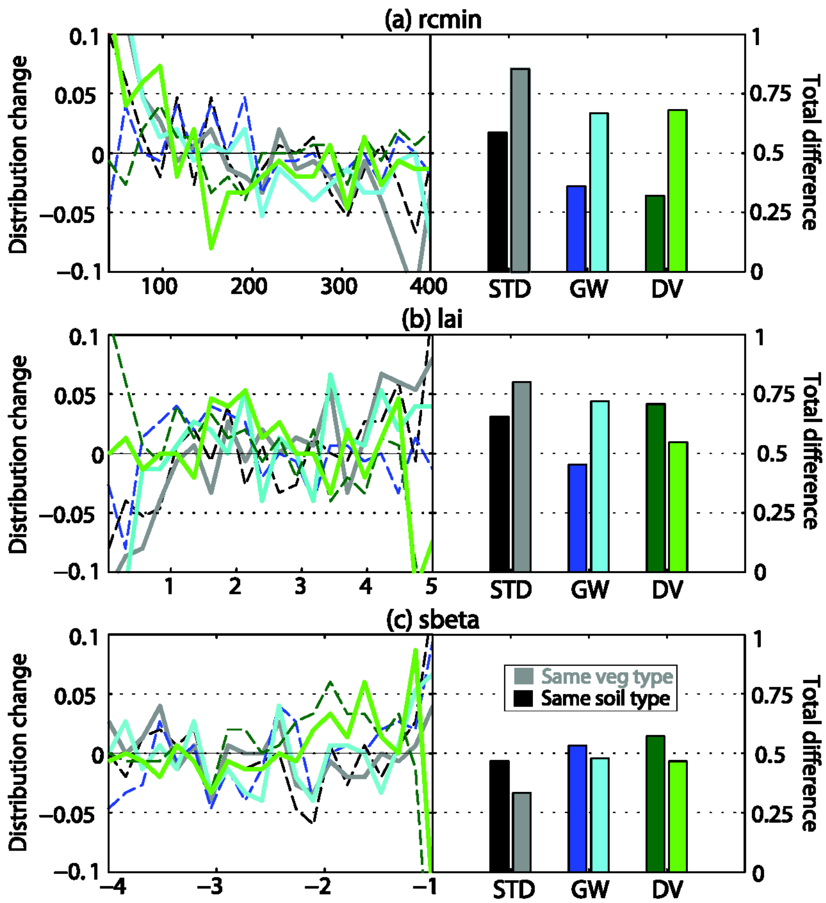

Figure 11. Comparison of the marginal posterior parameter distributions of selected, sensitive soil parameters: (a) maxsmc, (b) fxexp, and (c) czil. The total difference between parameter distributions at contiguous sites with the same soil type (Site 1 and 2) –sandy clay loam– (dashed, dark lines) is only sometimes smaller than the difference of distributions of the same parameters between sites with different meteorology (Site 2 and 8) (continuous, bright lines), which share the same vegetation cover type (grassland).

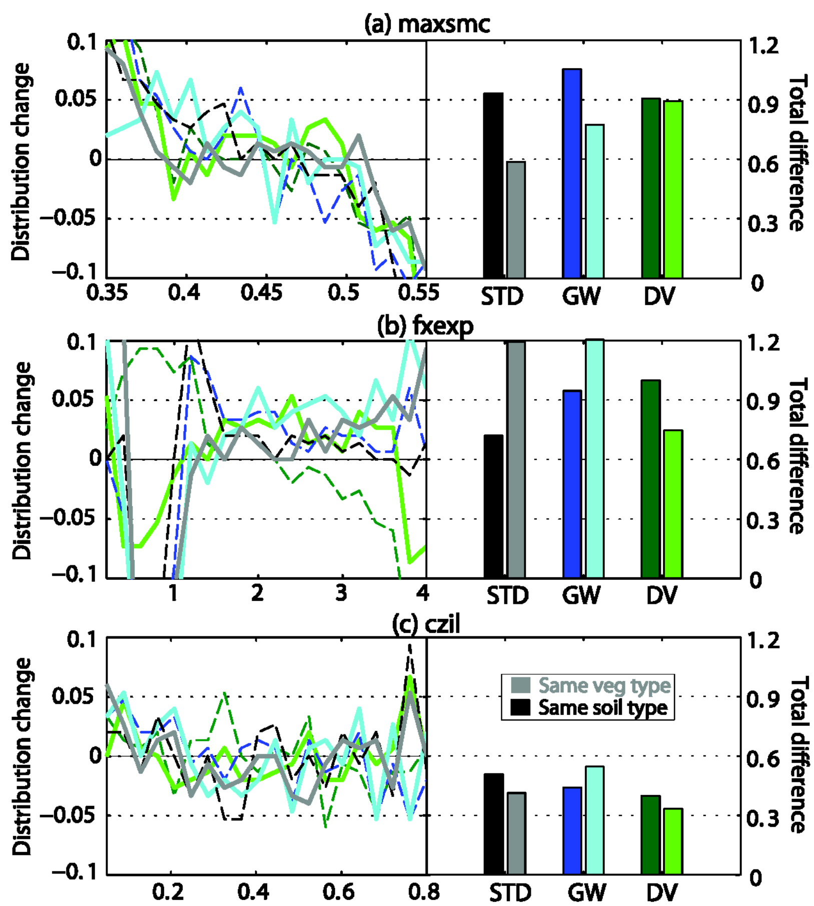

Figure 12. Clustering of sites using: (a) only the vegetation parameters of STD, (b) only the soil parameters of GW, and (c) both soil and vegetation parameters of GW. The similarity between marginal distributions of behavioral parameters at all sites is compared using different distances. The plots report the distance that maximizes the cophenetic correlation coefficient of the linkage. Note that neither soil nor vegetation parameters render groups solely based on soil or vegetation type. The clusters of all parameters seem to have a strong relationship with the 3 climatic zones: (1-3) semi-arid, (4-6) middling, and (7-9) semi-humid.

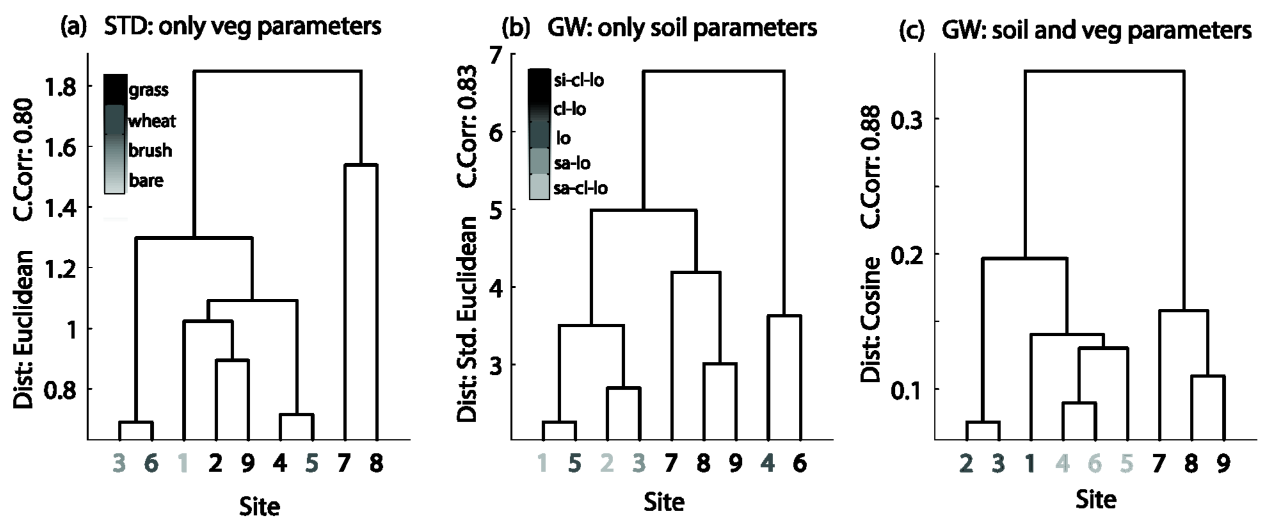

Figure 13. Clustering of soil (black), vegetation (gray) and GW-only parameters for the behavioral, marginal posterior distributions of (a) STD and (b) GW at all sites. The cophenetic correlation coefficient for the complete linkage for the parameters of STD and GW is 0.87 and 0.90, respectively. GW parameters seem to behave in a similar way as the soil parameters do.

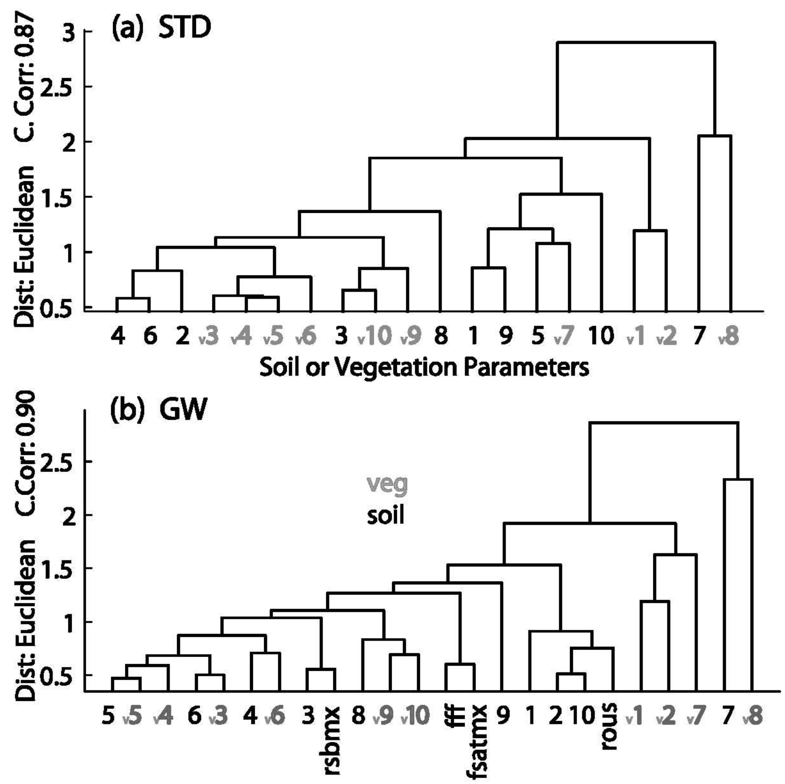

TABLES

Table 1. Average meteorology, near-surface states and turbulent fluxes observed during the calibration period (13 May - 25 Jun) at the nine IHOP_2002 sites. Indices of vegetation and soil classes are in parenthesis. Rainfall is cumulative over the observation period. Dry, sparsely vegetated sites (1-3) receive almost half of the amount of mean annual precipitation (MAP) than wet sites (7-9), with lush vegetation. Mean 2-m air temperature (Ta), sensible (H), latent (LE) and ground (G) heat flux, ground temperature (Tg) and soil moisture content at 5-cm (SMC_{5cm}).

Site	1	2	3	4	5	6	7	8	9
Lat (°N)	36.4728	36.6221	36.8610	37.3579	37.3781	37.3545	37.3132	37.4070	37.4103
Lon (°W)	100.6179	100.6270	100.5945	98.2447	98.1636	97.6533	96.9387	96.7656	96.5671
Vegetation type	bare ground (1)	grassland (7)	sagebrush (9)	pasture (7)	wheat (12)	wheat (12)	pasture (7)	grassland (7)	pasture (7)
Soil type	sandy clay loam (7)	sandy clay loam (7)	sandy loam (4)	loam (8)	loam (8)	clay loam (6)	silty clay loam (2)	silty clay loam (2)	silty clay loam (2)
Rain (mm)	154.5	69.1	72.4	164.5	173.6	203.6	175.4	296.6	250.8
MAP (mm)	530	540	560	740	750	800	900	880	900
Ta (°C)	21.4	21.7	22.5	20.7	20.7	21.0	20.7	20.1	19.9
H (Wm^{-2})	70.5	70.7	75.7	43.9	51.9	61.4	25.9	17.1	27.9
LE (Wm^{-2})	65.1	76.1	68.2	106.2	111.2	97.1	126.4	122.8	115.3
G (Wm^{-2})	-10.4	-6.4	-9.3	-2.7	-5.1	-7.5	-5.6	-12.1	-10.5
Tg (°C)	24.1	24.1	25.8	23.2	21.9	22.9	22.3	22.4	22.7
SMC_{5cm} (%)	15.4	18.0	7.0	18.0	18.1	19.0	33.2	32.8	34.0

Table 2. Feasible ranges of Noah-LSM parameters considered in the sensitivity analysis.

Parameter	Description	units	min	max
Soil parameters				
maxsmc	Maximum volumetric soil moisture	m^3m^{-3}	0.35	0.55
psisat	Saturated soil matric potential	$m\ m^{-1}$	0.1	0.65
satdk	Saturated soil hydraulic conductivity	$m\ s^{-1}$	1E-6	1E-5
b	Clapp-Hornberger b parameter	-	4	10
quartz	Quartz content	-	0.1	0.82
refdk	Used with refkdt to compute runoff parameter kdt		0.05	3
fxexp	Bare soil evaporation exponent	-	0.2	4
refkdt	Surface runoff parameter		0.1	10
czil	Zilintikevich parameter	-	0.05	8
csoil	Soil heat capacity	$Jm^{-3}K^{-1}$	1.26	3.5
Vegetation parameters				
rcmin	Minimal stomatal resistance	$s\ m^{-1}$	40	400
rgl	Radiation stress parameter used in F1 term of canopy resistance		30	100
hs	Coefficient of vapor pressure deficit term F2 in canopy resistance		36	47
z0	Roughness length	m	0.01	0.1
lai	Leaf area index	-	0.1	5
cfactr	Exponent in canopy water evaporation function	-	0.4	0.95
cmcmax	Maximum canopy water capacity used in canopy evaporation	m	0.1	2.0
sbeta	Used to compute canopy effect on ground heat flux	-	-4	-1
rsmax	Maximum stomatal resistance	$s\ m^{-1}$	2,000	10,000
topt	Optimum air temperature for transpiration	K	293	303
Dynamic Phenology parameters (Noah-DV only)				
fragr	Fraction of carbon into growth respiration	-	0.1	0.5
gl	Conversion between greenness fraction and LAI	-	0.1	1.0
rssoil	Soil respiration coefficient	s^{-1} x1E-6	0.005	0.5
tauhf	Average inverse optical depth for 1/e decay of light	-	0.1	0.4
bf	Parameter for present wood allocation		0.4	1.3
wstrc	Water stress parameter		10	400
xlaimin	Minimum leaf area index	-	0.05	0.5
sla	Specific leaf area	-	5	70
Groundwater parameters (Noah-GW only)				
rous	Specific yield	m^3m^{-3}	0.01	0.5
fff	e-folding depth of saturated hydraulic capacity	m^{-1}	0.5	10
fsatmx	Maximum saturated fraction	%	0	90
rsbmx	Maximum rate of subsurface runoff	ms^{-1} 1E-3	0.01	1

Table 3. Sensitive parameters according to a Kolmogorov-Smirnov test between samples that drive behavioral (multi-objectively calibrated) and non-behavioral simulations. 1 stands for sensitive, 0 for insensitive. The number of sensitive parameter is tabulated by class (soil, vegetation, and new GW or DV). See Table 1 for parameter names. No clear regional pattern of sensitivity can be readily discerned.

	Site	1			2			3			4			5			6			7			8			9		
	No. Par.	STD	GW	DV	STD	GW	DV	STD	GW	DV	STD	GW	DV	STD	GW	DV	STD	GW	DV	STD	GW	DV	STD	GW	DV	STD	GW	DV
soil parameters	1	1	1	1	1	1	1	1	1	1	1	1	1	0	1	1	1	1	1	1	1	1	1	1	1	1	1	1
	2	1	1	1	0	1	1	1	1	1	0	1	1	1	1	1	0	1	1	0	1	1	1	0	1	0	0	0
	3	1	0	1	0	0	1	0	1	1	1	0	1	1	1	1	0	1	1	1	0	0	1	1	0	0	1	0
	4	1	0	0	1	1	1	0	1	1	1	1	1	0	1	1	1	1	1	0	0	1	0	1	1	1	0	0
	5	1	1	0	0	1	0	1	1	1	1	1	1	1	1	1	1	1	1	1	0	1	1	1	1	0	1	1
	6	1	1	1	1	1	1	1	0	1	1	1	1	0	1	1	1	1	1	1	1	1	0	0	0	1	0	1
	7	1	1	1	1	1	1	1	1	1	1	1	1	1	1	0	1	1	1	1	0	0	1	1	0	1	0	1
	8	1	1	1	1	0	0	1	0	1	1	1	1	1	0	1	1	1	1	1	0	1	1	0	0	1	0	1
	9	1	0	1	1	1	1	1	0	1	1	1	1	1	0	1	0	0	1	1	1	1	1	1	1	1	1	1
	10	1	1	1	1	1	1	1	1	1	0	1	1	1	1	1	1	1	1	1	1	1	1	0	1	1	0	1
	#	10	7	8	7	8	8	8	7	10	8	9	10	7	8	9	7	9	10	8	5	8	8	7	6	7	4	7
vegetation parameters	1	1	0	1	1	1	1	0	1	1	1	1	1	1	1	1	1	1	1	1	1	1	1	1	1	1	1	1
	2	0	0	0	0	0	1	0	1	0	1	1	0	0	0	0	0	1	0	1	1	1	1	0	1	1	1	1
	3	0	0	1	1	0	1	1	0	1	1	1	1	0	0	1	0	1	1	0	0	0	0	0	1	0	0	0
	4	1	0	0	0	0	1	1	0	1	1	0	1	1	1	1	0	0	1	1	0	0	1	0	1	1	0	1
	5	1	1	1	1	1	1	0	0	1	0	1	1	1	1	1	1	1	1	1	1	1	1	1	0	1	1	1
	6	0	0	0	0	0	1	1	0	1	1	1	1	0	1	1	0	1	1	1	0	0	0	0	1	0	0	1
	7	1	1	1	0	1	1	1	0	1	1	1	1	1	1	1	1	1	1	0	1	1	0	1	0	1	1	1
	8	1	1	1	1	0	1	1	1	1	1	1	1	1	1	1	1	1	1	1	1	1	1	1	1	1	1	1
	9	0	1	0	1	0	0	0	0	1	1	1	0	0	1	1	0	1	1	1	0	1	0	1	0	1	0	1
	10	1	0	1	0	0	1	0	0	1	0	0	1	1	1	1	0	1	1	1	1	1	0	1	0	1	1	1
	#	6	3	6	5	3	9	5	3	9	8	8	8	6	8	9	4	9	9	8	6	7	5	6	6	8	6	9
new GW or DV parameters	1		1	1		1	0		1	1		1	1		1	1		1	1		0	1		1	1		0	1
	2		1	1		0	1		1	1		1	1		1	1		1	1		0	1		1	1		0	1
	3		1	0		0	1		0	0		1	1		1	1		1	1		1	0		0	0		0	0
	4		1	1		0	0		0	0		1	0		1	0		1	0		1	0		1	1		0	1
	5			0			1			1			1			0			0			0			1			1
	6			1			1			1			1			1			1			0			1			1
	7			1			1			1			1			1			1			1			0			0
	8			1			1			1			1			1			1			1			1			1
	#		4	6		1	6		2	6		4	7		4	6		4	6		2	4		3	6		0	6
	Total	16	14	20	12	12	23	13	12	25	16	21	25	13	20	24	11	22	25	16	13	19	13	16	18	15	10	22

Table 4. Spearman rank correlation coefficients between parameter sets belonging to the behavioral set for STD (up the diagonal) and GW (below the diagonal). Note the change in the covariance structure in Fig. 8. See Table 1 for abbreviations of parameter names.

	STD						
GW	maxsmc	psisat	satdk	fxexp	rous	fff	fsatmx
maxsmc		-0.10	-0.40	0.29			
psisat	-0.33		-0.14	-0.32			
satdk	-0.09	0.49		0.22			
fxexp	-0.26	0.41	0.23				
rous	-0.01	0.26	0.24	0.14			
fff	0.11	-0.46	-0.45	-0.49	-0.37		
fsatmx	-0.22	-0.04	-0.17	0.09	-0.37	0.17	
rsbmx	0.11	-0.25	-0.13	-0.21	0.32	0.08	-0.24

Table 5. Spearman rank correlation coefficients between parameter sets belonging to the behavioral set for STD (up the diagonal) and DV (below the diagonal). Note the change in the covariance structure in Fig 9. See Table 1 for abbreviations of parameter names.

	STD						
DV	rcmin	hs	maxsmc	psisat	fragr	bf	xlaimin
rcmin		-0.35	0.44	0.02			
hs	0.30		-0.15	-0.36			
maxsmc	-0.16	-0.29		-0.10			
psisat	0.50	0.36	-0.21				
fragr	0.58	0.24	-0.02	0.10			
bf	0.61	0.30	-0.19	0.59	0.40		
xlaimin	-0.72	-0.31	0.10	-0.31	-0.62	-0.54	
sla	0.80	0.21	-0.15	0.35	0.66	0.45	-0.67

LIST OF FIGURES

FIG 1. IHOP_2002 near-surface state and flux stations. The contours show the strong east - west mean annual precipitation (MAP) gradient. The nine sites were sited in representative land covers (see Table 1): six on grassland of varying thickness, two on winter wheat, one on bare ground, and one on shrubland. The surface temperature of the dry (MAP=550 mm), sparsely vegetated sites (1-3) is mainly linked to the soil moisture. In contrast, the green, lush vegetation of the wet sites (7-9) (MAP=900 mm) controls the surface temperature. In sites 4-6 (MAP=750 mm), a mix of winter wheat and grassland, the surface temperature is influenced by both soil moisture and vegetation.

FIG 2. (a) First-order Sobol' sensitivity indices for the parameters of STD, GW and DV at all sites. S_i stands for the individual contribution of a parameter to the variance of the RMSE of H. (b) Difference between Sobol''s total sensitivity index and S_i. S_{Ti} -S_i is the contribution to the variance through interactions with other parameters. Parameters grouped by soil and vegetation. Regional sensitivity patterns from semi-arid (MAP=550 mm), sparsely vegetated sites (1-3) to semi-humid (MAP=900 mm) sites (7-9) with green, lush vegetation, are easily distinguishable.

FIG 3. Same as Figure 2 but for LE.

FIG 4. Same as Figure 2 but for SMC_{5cm}.

FIG 5. Tradeoff LE-SMC_{5cm} and cumulative distribution functions (CDF) of scores of behavioral STD, GW and DV at Site 7. (a) Scatterplot in objective function space of parameter sets that maximize the likelihood function after multi-objective calibration against {H, LE, G, Tg, SMC_{5cm}}. CDF of root mean squared errors (RMSE) of behavioral runs evaluated against observed (b) LE, and (c) SMC_{5cm}. GW (dark grey), DV (light gray) perform as good as or better than STD (black).

FIG 6. Uncertainty ranges of the 150 ensemble members of behavioral runs of STD (black), GW (dark gray) and DV (light gray) at Site 7. (a) Average diurnal LE. (b) Hourly SMC_{5cm}. Plots show the interquartile range (50% of the runs) in continuous lines and the 90% confidence bounds (5% to 95% quantile) in dashed lines. Observations are shown with symbols. The spread of LE by STD is larger than that of DV, GW. The ensemble of GW shows wetter SMC_{5cm} than the rest.

FIG 7. Marginal cumulative distribution functions (CDF) of the posterior distribution of selected behavioral parameter sets at Site 7. (a) Porosity [maxsmc], (b) minimum stomatal resistance [rcmin], (c) maximum water holding capacity of the canopy [cmcmax], and (d) effect of the vegetation on ground heat flux [sbeta]. Along with the CDFS, the histograms and interquatile ranges are shown. The trend in the scatterplots of RMSE of LE and SMC_{5cm} is shown by fitting a minimum complexity polynomial. Note that in all subpanels GW (dark grey), DV (light gray) and STD (black) are shown.

FIG 8. Multivariate posterior distribution of the behavioral parameters of STD and GW at site 7 shown for selected parameter combinations in bivariate plots. Higher density of parameter values are indicated with increasingly redder contours. The response surface of SMC_{5cm} is shown in the back; darker regions have higher errors. The bi-modal behavior of GW is signaled by *m1* and *m2*. See text for explanation.

FIG 9. Bivariate depiction of the posterior distribution of behavioral parameters of STD and DV at Site 7. Higher density of parameter values are indicated with red contours. The response surface of LE is shown in the back; darker regions have higher errors. Note the significant change in the identifiability of hs and maxsmc.

FIG 10. Comparison of the marginal posterior parameter distributions of selected, sensitive vegetation parameters: (a) rcmin, (b) lai, and (c) sbeta. The total difference between parameter distributions at sites with the same vegetation cover type (Site 2 and 8) (continuous, bright lines) is not smaller than the difference of distributions of the same parameters between contiguous sites (Site 2 and 1) (dashed, dark lines), which share the same soil type.

FIG 11. Comparison of the marginal posterior parameter distributions of selected, sensitive soil parameters: (a) maxsmc, (b) fxexp, and (c) czil. The total difference between parameter distributions at sites with the same soil type (Site 5 and 7) (continuous, bright lines) is in general not smaller than the difference of distributions of the same parameters between contiguous sites (Site 5 and 6) (dashed, dark lines), which share the same vegetation cover type.

FIG 12. Clustering of sites using: (a) only the vegetation parameters of STD, (b) only the soil parameters of GW, and (c) both soil and vegetation parameters of GW. The similarity between marginal distributions of behavioral parameters at all sites is compared using different distances. The plots report the distance that maximizes the cophenetic correlation coefficient of the linkage. Note that neither soil nor vegetation parameters render groups solely based on soil or vegetation type. The clusters of all parameters seem to have a strong relationship with the 3 climatic zones.

FIG 13. Clustering of soil (black), vegetation (gray) and GW parameters for the behavioral, marginal posterior distributions of (a) STD and (b) GW at all sites. The cophenetic correlation coefficient for the complete linkage for the parameters of STD and GW is 0.87 and 0.90, respectively. GW parameters seem to behave in a similar way as the soil parameters do.

LIST OF TABLES